

UNIVERSIDADE DE SÃO PAULO
ESCOLA POLITÉCNICA

MARCO TIMICH

Process mineralogy of a lithium enriched pegmatite combining mineral separation
and SEM based automated mineralogy

São Paulo

2021

MARCO TIMICH

Process mineralogy of a lithium enriched pegmatite combining mineral separation
and SEM based automated mineralogy

Versão corrigida

Master's thesis presented to the
Escola Politécnica da Universidade
de São Paulo to obtain the degree of
Master of Science

Concentration area:
Mineral Engineering

Advisor:
Profa. Dra. Carina Ulsen

São Paulo


2021

Autorizo a reprodução e divulgação total ou parcial deste trabalho, por qualquer meio convencional ou eletrônico, para fins de estudo e pesquisa, desde que citada a fonte.

Este exemplar foi revisado e corrigido em relação à versão original, sob responsabilidade única do autor e com a anuência de seu orientador.

São Paulo, 19 de agosto de 2021

Assinatura do autor: Marco Timich

Assinatura do orientador: 

Catálogo-na-publicação

Timich, Marco

Process mineralogy of a lithium enriched pegmatite combining mineral separation and SEM based automated mineralogy / M. Timich -- versão corr. -- São Paulo, 2021.

76 p.

Dissertação (Mestrado) - Escola Politécnica da Universidade de São Paulo. Departamento de Engenharia de Minas e de Petróleo.

1.mineralogia de processo I.Universidade de São Paulo. Escola Politécnica. Departamento de Engenharia de Minas e de Petróleo II.t.

Name: TIMICH, Marco

Master thesis: Process mineralogy of lithium enriched pegmatite samples combining mineral separation and SEM based automated mineralogy

Master's thesis presented to the Escola
Politécnica da Universidade de São
Paulo to obtain the degree of Master of
Science

Approved in:

Major committee

Prof. Dr. Prof. Dra. Carina Ulsen

Instituição: Escola Politécnica - USP

Julgamento: Aprovado

Prof. Dr. Dr. Reiner Neumann

Instituição: Centro de Tecnologia Mineral (CETEM)

Julgamento: Aprovado

Prof. Dr. Dr. Paulo Fernando Almeida Braga

Instituição: Centro de Tecnologia Mineral (CETEM)

Julgamento: Aprovado

AGRADECIMENTOS

Em primeiro lugar agradeço à minha orientadora, Professora Doutora Carina Ulsen, por todo empenho e sentido prático com que me orientou neste trabalho e em todas as atividades que realizei durante o mestrado.

Desejo igualmente agradecer a todos os meus amigos em especial ao Renato Contessotto, Daniel Uliana, Guilherme Nery, Julia Guerra, Juliana Livi, Saulo Colenci, Thais Borttotti, Gaspar Darin, Gislayne Kelmer, Ilda, Ana Carolina, Jhonatan Florez, Manuela, Ingled, Lino, Juscelino, Erilio, Adhemar, Alicia, Mariana, Mavinieur cuja simples presença já se traduziu em apoio por diversas vezes.

Também agradeço à minha companheira Thereza Yogi, que não mediu esforços para me apoiar, sempre.

Agradeço à toda equipe do Laboratório de Caracterização Tecnológica e a todos os funcionários do departamento de Engenharia de Minas da EPUSP que eu tive o prazer de conhecer.

À minha família que me possibilitou estar aqui e que não tenho palavras para agradecer e explicitar minha total admiração. Obrigado!

Agradeço à Coordenação de Aperfeiçoamento de Pessoal de Nível Superior (CAPES) pelo apoio na realização do presente trabalho.

RESUMO

Existem duas fontes principais de lítio, as salmouras - localizadas principalmente no Chile, Argentina e Bolívia - e as pegmatitos que ocorrem disseminadas no mundo e correspondem a mais de 50% da produção de lítio. Com o aumento da demanda global de lítio, os depósitos em pegmatito tornam-se cada vez mais atrativos e viáveis economicamente. A reserva de lítio no Brasil é encontrada exclusivamente em pegmatitos e corresponde a menos de 1% das reservas mundiais lítio, mas um estudo recente aponta para a existência de uma quantidade expressiva de reservas no Brasil, podendo alcançar 8% das reservas mundiais. Este trabalho relata um estudo de caracterização tecnológica realizado em 10 amostras oriundas de um depósito pegmatítico do sudeste de Minas Gerais. Estudos de mineralogia quantitativa baseada em MEV-EDS, aliados a análises químicas (FRX, ICP-OES, LA-ICPMS) e mineralógicas (DRX), mostram que o espodumênio (8,0% em massa de Li_2O) é o principal portador de lítio, mas este também ocorre em micas, como muscovita (0.5% em massa de Li_2O) e lepidolita (3.1% em massa de Li_2O). A caracterização do concentrado de espodumênio ($d=3.11$) obtido por líquido denso ($d=2.95$) mostrou duas tendências nas amostras: a) amostras com baixa distribuição de lítio no produto afundado (~44%) com teor de Li_2O elevado (~6.5% em massa) e b) amostras com alta distribuição de lítio no produto afundado (58%) e menor teor de Li_2O (~4.9% em massa) neste produto. A menor distribuição de lítio no produto afundado foi associada ao maior conteúdo modal de lepidolita, pois esta se reporta ao produto flutuado. A recuperação mais alta de lítio foi associada com menor teor modal de lepidolita e o menor teor de Li_2O se deve à presença de minerais portadores de ferro (epídoto e anfibólio) que têm densidade semelhante ao espodumênio e, portanto, reportam ao produto afundado. O grau de liberação do espodumênio é maior que >88% e similar em todas as amostras, portanto não influenciou nos resultados de recuperação mássica do líquido denso. Este trabalho destaca a caracterização tecnológica como suporte ao beneficiamento mineral, especialmente na identificação de diferentes minerais portadores de lítio e sua partição como ferramenta de mineralogia de processo.

Palavras-chave: Mineralogia de processo, espodumênio, lítio

ABSTRACT

Brines located in Chile and Argentina are the main lithium reserve, however over 50% of lithium production comes from pegmatites distributed around the world. With the increase in lithium demand driven by its applications in energy storage technologies, pegmatite deposits become increasingly economically viable. Lithium's reserve in Brazil is found exclusively in pegmatites and accounts for less than 1% of global reserves, but a recent study indicates that Brazil can reach up to 8% of global reserves. This paper reports process mineralogy studies performed in 10 samples from a lithium pegmatite deposit from southeastern of Minas Gerais state in Brazil. Samples characterization were carried out combining heavy liquid separation and X-ray based automated mineralogy using Mineral Liberation Analyzer system (MLA) allied to XRF, ICP-OES, XRD and LA-ICPMS. Results showed that besides spodumene (8.0 wt% Li_2O), there are other lithium-bearing minerals, as muscovite (0.5 wt% Li_2O) and lepidolite (3.1 wt% Li_2O). The characterization of the spodumene ($d=3.11$) concentrate obtained by heavy liquid separation ($d=2.95$) revealed that samples present two main trends a) –samples with low lithium distribution in the sink product (~44%) with higher Li_2O grade (~6.5 wt%) and b) –samples with higher lithium distribution in the sink product (58%) with lower Li_2O content (~4.9 wt%). Lower lithium distribution in sink product is associated with higher modal content of micas since they carry lithium to the floated product. Lower lithium grade is related to the presence of iron-bearing minerals (e.g., epidote and amphibole), since they report to the sink product and do not contain Li. The liberation degree of spodumene is high and similar in all samples, therefore it did not influence distribution results. This work highlights the use of scanning electron microscopy (SEM) based automated mineralogy combined with other techniques in process mineralogy studies to guide mineral processing. Besides mineralogy and liberation characteristic, especially important was identifying lithium-bearing minerals and determining lithium's department.

Keywords: Process mineralogy, spodumene, lithium

FIGURE LIST

Figure 1 - World reserves and mine production in percentage (JASKULA, 2020).	17
Figure 2 - Estimated world lithium production and consumption (HOCKING et al., 2016; TADESSE et al., 2019).....	18
Figure 3 - Main lithium uses in 2019 in relative percentages (JASKULA, 2020).	19
Figure 4 - Greenbushes spodumene processing flowsheet (modified from BALE; MAY, 1989; GIBSON; AGHAMIRIAN; GRAMMATIKOPOULOS, 2017).....	23
Figure 5 - Mine site map showing the relative geographic location of the boreholes and samples.....	27
Figure 6 - Flowsheet of the experimental procedure of the broad mineral characterization. .	30
Figure 7 – Bulk sample XRD patterns.....	35
Figure 8 - MLA mineral composition maps showing liberated spodumene and gangue minerals in the -0.30 + 0.037 mm size fraction for all ten samples: a – MT01, b – MT02, c – MT03, d – MT04, e – MT05, f – MT06, g – MT07, h – MT08, I – MT09, j – MT10.....	39
Figure 9 - Size distribution of spodumene grains (ECD).	40
Figure 10 - Mine site map showing the geographic layout of the groups.....	45
Figure 11 - Bulk Li ₂ O wt% content in samples (a) and spodumene content in the -0.30 + 0.037 mm size fraction (b).....	45
Figure 12 - Lithium deportment in the density separation test.	46
Figure 13 - Cumulative weight and elemental distributions by size fractions.....	48
Figure 14 - Modal mineralogy of MLA measurements for Group 1 (a) and Group 2 (b).....	50
Figure 15 - Comparison of sample chemistry calculated by MLA and measured by XRF* for G1 (a) and G2 (b).	51
Figure 16 - MLA mineral composition map showing liberated spodumene and gangue minerals grains in the +0.15 mm size fraction for Group 1 (a, c, e). The mineral maps on the right-hand side show close up of the different mineral textures in some spodumene grains (b, d, f).	52
Figure 17 - MLA mineral composition map showing liberated spodumene and gangue minerals grains in fraction -0.21+0.15 mm for Group 2 (a. c. e). The mineral maps on the right-hand side show close up of the different mineral textures in some of the spodumene grains (b. d. f)....	53

Figure 18 - Spodumene liberation characteristics for Group 1 (a) and Group 2 (b). Liberation is based on spodumene area (liberated \geq 95% spodumene). Binary particles are composed of spodumene and another mineral phase and complex particles are composed of spodumene and two or more different mineral phases.....	56
Figure 19 - Mineral liberation by free surface area for spodumene in G1 (a) and G2 (b).....	57
Figure 20 - MLA mineral composition map of a mica particle showing the classification and the differences in X-ray spectra (a).BSE image and EDS analysis results table (b).	61
Figure 21 - Comparison of sample chemistry by size fraction calculated by MLA and measured XRF* for the floated products of Group 1 (a) and Group 2 (b).	63
Figure 22 - Modal mineralogy by size fraction of the floated products for Group 1 (a) and Group 2 (b).....	64
Figure 23 - Li ₂ O department in the Total +0.037 mm size fraction.....	65
Figure 24 - Li ₂ O department by size fractions in Group 1 (a) and in Group 2 (b).....	65
Figure 25 - Theoretical grade recovery curve for spodumene mineral grains in all studied size fractions of Group 1.....	66
Figure 26 - Theoretical grade recovery curve for spodumene mineral grains in all studied size fractions of Group 2.....	66
Figure 27 - Li ₂ O, Fe ₂ O ₃ and CaO content in Group 1 and Group 2.	67
Figure 28 - Li ₂ O, Fe ₂ O ₃ and CaO content in Total +0.037 mm size fraction of Group 1 and Group 2 (a). Li ₂ O distribution in the Total +0.037 mm and -0.037 mm size fractions for both Groups (b).....	68
Figure 29 - Lithium distribution in the density separation test.	69

TABLE LIST

Table 1 - Lithium deposit types and some global examples (modified from BROWN et al., 2016).....	15
Table 2 - Common lithium-bearing minerals found in pegmatites and their characteristics. ..	16
Table 3 - Main minerals and typical metallurgical results for some processing plants (BALE; MAY, 1989; BROWN et al., 2016; BULATOVIC, 2015; TADESSE et al., 2019).	23
Table 4 - MLA measurement procedure.	32
Table 5 - Bulk chemical analysis.	33
Table 6 - Mineralogical composition of the -0.30+0.037 mm size fraction.	34
Table 7 - Chemical analysis by size fraction of the ten samples.....	37
Table 8 – Density separation results for the -0.30 + 0.037 mm size fraction in all ten samples.	42
Table 9 - Bulk chemical analysis.	46
Table 10 - Sieve size analysis for group 1 and group 2.	49
Table 11 - Association characteristics of spodumene in Group 1.	54
Table 12 - Association characteristics of spodumene in Group 2.	55
Table 13 – Density separation test results for Group 1.	58
Table 14 - Density separation test results for Group 2.	60
Table 15 - Average composition of muscovite grains obtained by LA-ICPMS.	62
Table 16 - Average composition of lepidolite grains obtained by LA-ICPMS.....	62

SUMMARY

1	INTRODUCTION	13
1.1	AIM OF THE THESIS	14
2	BACKGROUND	15
2.1	Geology of lithium	15
2.1.1	Continental Brines	15
2.1.2	Pegmatite	16
2.2	Market outlook	16
2.3	Applications	18
2.4	Spodumene beneficiation	19
2.4.1	Ore sorting	20
2.4.2	Dense media separation	20
2.4.3	Flotation	21
2.4.4	Magnetic Separation	22
2.5	Processing plant examples	22
2.6	Process Mineralogy of lithium	24
3	MATERIALS AND METHODS	27
3.1	Broad ore characterization	28
3.2	Combined samples	28
3.3	Detailed process mineralogy	29
3.4	Analytical techniques	30
3.4.1	Chemical Analysis	30
3.4.2	XRD	31
3.4.3	SEM based automated mineralogy	31
3.4.4	LA-ICPMS	32
4	RESULTS	33
4.1	Broad ore characterization	33

4.1.1	Bulk chemical analysis	33
4.1.2	Assessment of mineral content	33
4.1.3	Sieve analysis.....	35
4.1.4	Spodumene characteristics	36
4.1.5	Mineral density separation.....	40
4.2	Combined samples.....	44
4.3	Detailed process mineralogy.....	46
4.3.1	Chemical Analysis	46
4.3.2	Sieve analysis.....	46
4.3.3	Mineral Composition	50
4.3.4	Spodumene Characteristics.....	51
4.3.5	Mineral Density Separation.....	57
4.3.6	Mica compositions.....	61
4.3.7	Lithium deportment	64
4.3.8	Grade-recovery.....	65
5	DISCUSSION	67
6	CONCLUSION.....	71
7	BIBLIOGRAPHY	72

1 INTRODUCTION

In 2020, lithium has been added for the first time to the list of Critical Raw Materials of the European commission. The document states that Europe will need up to 18 times more lithium in 2050 to supply the demand of electric vehicles batteries and energy storage systems (EUROPE, 2020)

In Brazil, the Ministry of Mines and Energy (MME) launched the national mining plan to 2030 to guide the development of the mining sector over the future years and sets lithium as a strategic mineral for the future. Therefore, studies with lithium pegmatites can contribute for the technological development of the mining sector and the country. Also, a recent publication of the Brazilian Geological Survey which assessed the lithium potential in Brazil, stated that the country could reach approximately 8% of the global lithium reserve, with more than 1Mt of Li_2O (PAES et al., 2016). Currently Brazilian reserves account for less than 1% of global lithium reserves.

As seen, lithium has become a metal of crucial importance and therefore its demand rapidly increases, mainly due to its use in green energy storage technologies (KAVANAGH et al., 2018). The rising demand of the metal requires an extensive knowledge of its uses and sources in order to maximize the use of the material (MARTIN et al., 2017).

Minerals present in pegmatitic rocks are one of the main sources of lithium, spodumene being the most important lithium-bearing mineral. To characterize such samples, besides mineralogical and liberation characteristics, a comprehensive understanding of the deportment of lithium between lithium-bearing minerals (e.g. spodumene and micas) is of crucial importance, especially when minerals show distinct physical properties. This impact directly in the interpretation of lithium data from whole rock analyses. However, it is not a simple task because lithium is not detected by the most usual analytical techniques and therefore, research in literature is scarce (SWEETAPPLE; TASSIOS, 2015). Some authors have tackled the problem combining automated mineralogy with other analytical techniques that are able to detect lithium, such as LA-ICPMS (ASSUMPÇÃO, 2015; AYLMORE et al., 2018a, 2018b; GRAMMATIKOPOULOS et al., 2021; SANDMANN; GUTZMER, 2013).

In this work, a combination of analytical techniques with laboratory mineral separation and scanning electron microscopy (SEM) based automated mineralogy have been used to characterize a spodumene pegmatite from southeastern Minas Gerais, Brazil. Since conventional SEM-EDS systems do not detect lithium, LA-ICPMS was used to determine the element content in all lithium-bearing minerals. This effort is of great importance because having an understanding of lithium's deportment is important to predict the response of ore reserves to metallurgical treatment options (AYLMORE, 2018). It is stated that ore deposits where lithium is present at >10% in other phases than spodumene are more economically challenging because of the lower "head" grade after the unwanted minerals are eliminated (J. WELHAM, 2019).

1.1 Aim of the master's thesis

The assessment of lithium enriched pegmatite samples using a combination of analytical techniques to determine mineral associations and liberation characteristics of spodumene is the aim of this dissertation. Also, search for secondary lithium-bearing minerals, quantify their lithium content to determine lithium deportment and its implication in mineral processing. To evaluate the separability of spodumene from other lithium-bearing minerals and iron oxides that can be detrimental to the spodumene concentrate or further beneficiation, is of interest. Results may facilitate further mineral processing developments and aid maximizing economic use of the raw material. Nonetheless throughout the work, secondary products of lithium and other elements, such as rubidium, will be highlighted.

2 BACKGROUND

2.1 Geology of lithium

Lithium is a relatively rare element, although it is found in many source types, but always in low concentrations (GARRETT, 2004). The average lithium content in the upper crust is commonly cited as being 20 ppm (MCLENNAN, 2001; VINE, 1976).

Currently the main lithium sources are continental brines and minerals found in rocks called pegmatites. Future sources are likely to include lithium-bearing clays, such as hectorite and jadarite, oilfield and geothermal brines. Table 1 shows examples of lithium deposits around the world and their typical lithium content.

Table 1 - Lithium deposit types and some global examples (modified from BROWN et al., 2016).

Deposit type		Typical Li ₂ O content (wt%)	Examples
Mineral	Pegmatite	1.5-4	Greenbushes (Australia)
	Hectorite	0.4	Kings Valley, Nevada
	Jadarite	1.5	Jadar, Sérvia
Brine	Continental	0.04-0.15	Atacama (Chile)
	Geothermal	0.01-0.035	Salton Sea Area, California
	Oilfields	0.01-0.05	Smackover Oilfield, Arkansas

2.1.1 Continental Brines

Lithium continental brine deposits are endorheic basins in which high solar evaporation rates increases lithium concentration. These deposits typically contain salt and often produce potassium and boron as by products. The most notable continental brine deposits are in located a region called Lithium Triangle, located in the center of Andes Mountains. This area lies in a plateau called Altiplano-Puna between the cities of Chile and Argentina. These cities together have more than 50% of lithium's global reserves (EVANS, 2014).

The beneficiation process involves pumping the brine into man-made ponds, where solar evaporation progressively concentrates the brine in lithium and precipitates other salts. The brine is transferred through a series of ponds and in each pond different salts are removed, initially halite is precipitated, then sylvite, and others.

When the brine reaches approximately ~6% Lithium chloride concentration. At this point, lithium is removed as lithium carbonate and lithium chloride (TRAN; LUONG, 2015).

2.1.2 Pegmatite

Pegmatites are igneous rocks, mostly of granitic compositions that distinguish from other igneous rocks by its extremely coarse but variable grain size. They typically form lenses, dykes or veins with spatial zonation of mineral assemblages, including monomineralic zones (LONDON, 2018). According to the chemical composition, pegmatites are divided into two 'families'; the NYF family (containing niobium, yttrium and fluorine) and the LCT family (containing lithium, cesium and tantalum) (CERNY; ERCIT, 2005).

LCT pegmatites typically contain 12 to 30% spodumene, 22 to 27% quartz, 30 to 50% feldspar, and 3 to 5% mica and accessory minerals, such as cassiterite and columbite (KAVANAGH et al., 2018). Spodumene, a lithium-aluminum silicate, is the most common lithium-bearing mineral. Other minerals less common or with less lithium content that may also be present in these pegmatites are petalite, lepidolite and amblygonite (MESHRAM; PANDEY; MANKHAND, 2014). Table 2 lists the main lithium-bearing minerals found in pegmatites along with their composition, theoretical Li₂O content and specific gravity (s.g.).

Table 2 - Common lithium-bearing minerals found in pegmatites and their characteristics (BROWN et al., 2016).

Mineral	Formula	Theoretical Li ₂ O content (wt%)	s.g.
Spodumene	LiAl[SiO ₃] ₂	8.1	3.1-3.2
Petalite	LiAlSi ₄ O ₁₀	4.9	2.4-2.5
Lepidolite	KLiAl ₂ Si ₃ O ₁₀ (OH,F) ₃	6.0	2.8-2.9
Amblygonite	LiAl[PO ₄][F,OH]	10	3.0-3.2
Zinnwaldite	K[Li.Al.Fe] ₃ [Al.Si] ₄ O ₁₀ [F.OH] ₂	4.1	2.9-3.2
Eucryptite	LiAlSiO ₄	12	2.67

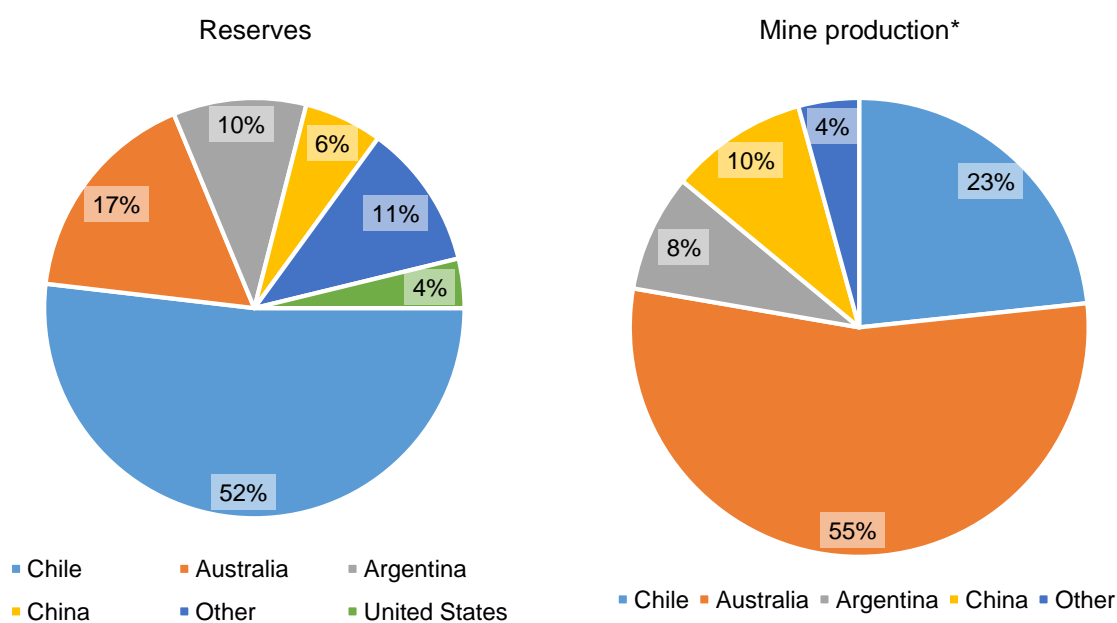
2.2 Market outlook

Until the 1980s lithium was mainly extracted from pegmatites, but with the start of lithium production from lithium enriched brines with cheaper prices, companies

operating in pegmatite deposits could not compete (GRUBER et al., 2011). Since lithium is being considered a strategic resource due to its applications in green energy storage technologies, its price has risen substantially, permitting lithium pegmatite deposits to become economically viable again (LI; EKSTEEN; KUANG, 2019).

Currently approximately 70% of world's lithium reserves is found in brines, mainly located between Chile and Argentina, and 25% in pegmatites mainly located in Australia (Figure 1), the remaining 5% are found in clays, geothermal waters, and oil field brines. In terms of lithium production, approximately 60% comes from pegmatite deposits, mainly from Australia, other producers with smaller contributions are Canada, Zimbabwe, Portugal, and Brazil. Brines account for approximately 40% of the global lithium production and the major producers are Chile and Argentina (Figure 1) (JASKULA, 2020).

Figure 1 - World lithium reserves and mine production in percentage (JASKULA, 2020).

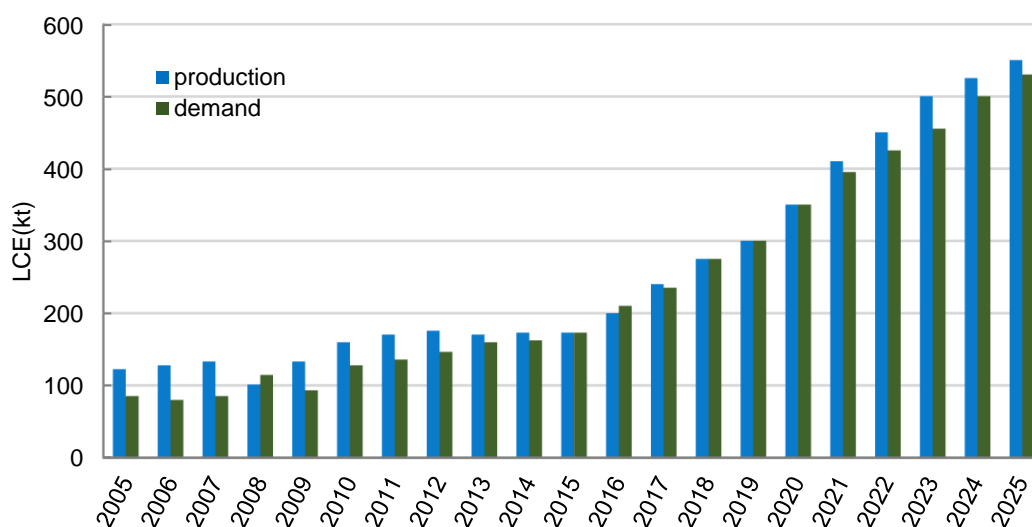


*excluding United States

Figure 2 shows the world lithium production and consumption between 2005 and 2025, the lithium amount is expressed as Lithium Carbonate Equivalent (LCE) which is a terminology often used due to its importance in terms of produced volume. The trend suggests that production and demand increased approximately 10% yearly since 2015 and tends to keep this pace until 2025. The optimistic scenario estimates

that demand will be approximately 550 LCE Mt by 2025, driven mainly by the large scale insertion of electric vehicles in the automobile market (HOCKING et al., 2016; JASKULA. 2019; MARTIN et al., 2017).

Figure 2 - Estimated world lithium production and consumption (HOCKING et al., 2016; TADESSE et al., 2019).



*LCE: Lithium Carbonate Equivalent (0.188% Li)

In Brazil, lithium occurrences are associated with pegmatite located in the states of Minas Gerais, Ceará, Rio Grande do Norte, and Paraíba. Some pegmatite are known since 1924, but commercial exploitation started in 1966 in spodumene pegmatites from Araçuaí, in Minas Gerais (NASCIMENTO et al., 2008). The lithium reserve in Brazil is estimated in 287.500 LCR(t) and resource in 960.000 LCE(t) (JASKULA, 2019).

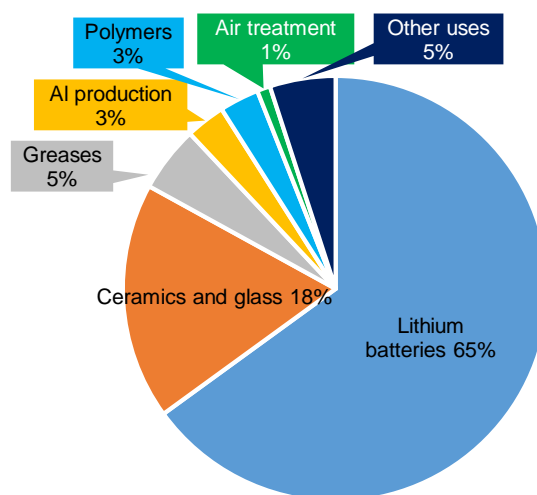
2.3 Applications

The physical and chemical properties of lithium minerals and lithium compounds grant them a great variety of applications in the industry. The direct use of lithium mineral concentrates (mainly spodumene) is limited to glassmaking and the production of ceramics (CHRISTMANN et al., 2015), in 2019 the estimated global end use of these products was 18% of lithium's market share (Figure 3) (JASKULA, 2020). The addition of lithium to glasses increases hardness and reduces thermal expansion, while in the ceramic industry it lowers the melting temperature and also reduces thermal expansions in the resulting ceramic product (GARRETT, 2004).

When used in the form of compound, lithium is mostly applied in manufacturing of Li-ion batteries. Since lithium is the most electropositive of all metals, it can generate the greatest electrical power per unit weight of any metal. Currently batteries are ranked first among the global end use of lithium market share, accounting for approximately 65% (Figure 3) (JASKULA, 2020). Other applications of lithium compounds include high-performance lubricant greases, humidity reducers, air coolers in air conditioning systems, drugs to control bipolar disorders and production of tritium for nuclear weapons (GARRETT, 2004).

The lithium compounds produced in Brazil are currently not suitable for battery grade materials. Applications are restricted to more conventional uses such as greases and lubricants. Approximately 90% of lithium compounds are used in grease and 10% used in ceramics, drugs and other uses (GARCIA, 2015).

Figure 3 - Main lithium uses in 2019 in relative percentages (JASKULA, 2020).



2.4 Spodumene beneficiation

Depending on the intended end use, the processing of spodumene aims to achieve either technical-grade or chemical-grade lithium concentrates. The former is used in ceramic and glass applications and the latter in several applications, but mainly in Li-ion batteries manufacture.

Factors such as the impurities in the spodumene crystal structure (mainly iron) and the size distribution can be limiting in obtaining the desired type of concentrate.

The purity specifications for technical grade spodumene concentrates require a coarser concentrate with high Li_2O content and relatively low gangue mineral content. Chemical grade spodumene concentrate specifications are less restrictive making it easier to obtain higher processing recoveries (GIBSON; AGHAMIRIAN; GRAMMATIKOPOULOS, 2017).

For example, specifications for technical grade spodumene concentrate from Albemarle are: Li_2O content $\geq 6.5\%$, Fe_2O_3 content $\leq 0.1\%$ and grain size of $100\% < 500 \mu\text{m}$, max. $18\% > 212 \mu\text{m}$ and min. $60\% > 75\%$ (ALBEMARLE, 2017). Generic specifications for chemical grade spodumene concentrate are: Li_2O content $> 6.0\%$ and Fe_2O_3 content $< 1-1.5\%$ (OLIAZADEH et al., 2018).

The processing methods available to achieve separation of spodumene and gangue minerals are ore sorting, dense media separation (DMS), magnetic separations and froth flotation (OLIAZADEH et al., 2018; TADESSE et al., 2019).

2.4.1 Ore sorting

Ore sorting reduces mine dilution by removing amphibole and pyroxene prior to the beneficiation plant feed. Since these minerals are common in gangue rocks of lithium-bearing pegmatite ores, it is ideal to reject them at an early stage in process because they tend to interfere with both DMS and spodumene flotation operations, and can be difficult to separate from spodumene (OLIAZADEH et al., 2018).

Since the working range of ore sorters is limited to $+12.5 \text{ mm}$ they are usually installed after the crushing plant. Therefore, to be effective in rejecting iron minerals and silicates (pyroxene, amphibole, epidote) and improving lithium head grade, liberation of these grains in coarse fractions is necessary (OLIAZADEH et al., 2018).

2.4.2 Dense media separation

Dense media separation (DMS) is a pre-concentration technique that benefits processing by reducing feed amount prior to grinding and flotation and, consequently, decreasing energy consumption and operation costs (GIBSON; AGHAMIRIAN; GRAMMATIKOPOULOS, 2017).

The technique is applied prior to grinding for final liberation to reject gangue minerals (GIBSON; AGHAMIRIAN; GRAMMATIKOPOULOS, 2017). Spodumenes

specific gravity (s.g. = 3.1 – 3.2) is slightly different as compared to that of the major silicate gangue minerals present in pegmatite ores, such as quartz, feldspar (s.g. ~ 2.6) and micas (s.g. = 2.8 – 3.0), this makes the separation challenging but possible in most cases. However, amphibole, pyroxene, garnet, and epidote group minerals have similar specific gravity to spodumene and, therefore, deport to the DMS concentrate with spodumene (GIBSON; AGHAMIRIAN; GRAMMATIKOPOULOS, 2017). Other factors that can affect DMS efficiency are the mineralogical transformation of spodumene to micaceous and clay minerals that reduces its specific gravity and the tendency of spodumene to break into acicular particles which become buoyant (MUNSON; CLARKE, 1955).

The DMS circuit usually includes two stages at different dense media specific gravities: the first at a lower specific gravity (~2.7) to reject silicate gangue, and the second at higher specific gravity (~2.9) to produce a high-grade spodumene concentrate. DMS is typically carried out on the -850+500 μm fraction, however, it is noteworthy that spodumene needs a high degree of liberation for its effective concentration and recovery. Poor spodumene liberation may result in significant lithium losses to the float product and impinge the use of DMS in processing (GIBSON; AGHAMIRIAN; GRAMMATIKOPOULOS, 2017).

2.4.3 Flotation

Flotation is widely used in processing of spodumene pegmatite ores where the average particle size or difference in specific gravities between gangue minerals is too small for efficient separation (TADESSE et al., 2019). The flotation concentrate must be suitable for downstream operations such as hydrometallurgical processing (OLIAZADEH et al., 2018).

Several flotation flowsheet options can be selected depending on the nature of the gangue minerals present (BULATOVIC, 2015; GIBSON; AGHAMIRIAN; GRAMMATIKOPOULOS, 2017; OLIAZADEH et al., 2018). The main options are:

- A. Spodumene flotation only;
- B. Gangue preflotation (mica) followed by spodumene flotation;
- C. Gangue preflotation (mica) followed by spodumene flotation and then feldspar flotation from spodumene flotation tailing;

- D. Split of spodumene flotation into coarse particle flotation and fine particle flotation.

2.4.4 Magnetic Separation

Magnetic separations is used to separate iron-bearing minerals, such as amphibole and tourmaline, from spodumene concentrates. Although it can be used prior to flotation, to remove large quantities of iron-bearing minerals, it is most common to perform after flotation, to produce a low iron content concentrate, suitable for ceramics and glass manufacture (GIBSON; AGHAMIRIAN; GRAMMATIKOPOULOS, 2017; TADESSE et al., 2019).

2.5 Processing plant examples

Table 3 shows a summary of typical ore and gangue minerals and the metallurgical performance of some selected plants. The Greenbushes Lithium Operations, located in Western Australia, is a major producer of lithium concentrate globally. The Kings Mountain plant, located in North Carolina (USA) is considered one of the three largest lithium-bearing pegmatite deposits in the world, together with Manono deposit in the Democratic Republic of Congo and Greenbushes. The Bernic Lake group of pegmatites in Manitoba (Canada) are complex zoned pegmatites with over 100 different minerals including spodumene, lepidolite, amblygonite and eucryptite (BROWN et al., 2016). The Bikita pegmatite, located in Zimbabwe, is one of the world's largest lithium deposits and contains several lithium minerals including spodumene, petalite, lepidolite, eucryptite and amblygonite (VON KNORRING; CONDLIFFE, 1987). The Bald Hill lithium-tantalum mine, located in Australia, started production of spodumene concentrate in early 2018, tantalite is a major by-product (TADESSE et al., 2019).

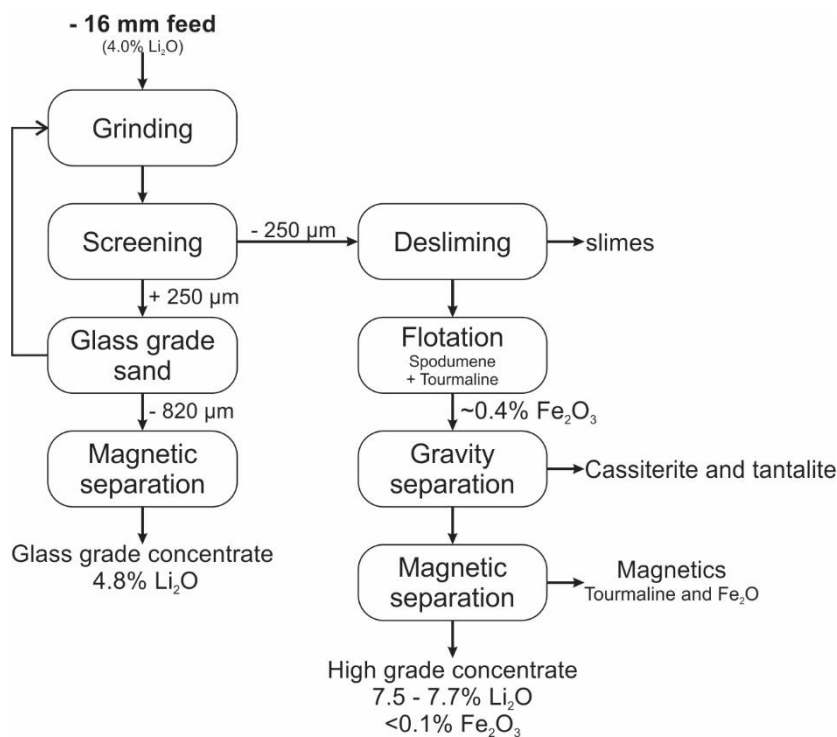
As an example, Figure 4 shows a simplified flowsheet of the Greenbushes spodumene processing plant. The plant produces technical and chemical grade lithium concentrates, using spiral circuit, shaking table, heavy media, flotation and magnetic processes to upgrade the ore (BALE; MAY, 1989; GIBSON; AGHAMIRIAN; GRAMMATIKOPOULOS, 2017).

Table 3 - Main minerals and typical metallurgical results for some processing plants (AMG, 2017; BALE; MAY, 1989; BROWN et al., 2016; BULATOVIC, 2015; CBL, 2016; TADESSE et al., 2019).

Plant	Main Minerals	Main gangue	Feed Li ₂ O wt%	Conc. Li ₂ O wt%	Beneficiation method
Greenbushes, Australia	Spodumene, cassiterite, tantalite	Tur	4.0	7.5-7.7	Flot/M.S./S.T.
Kings Mountain, USA	Spodumene	Alb, qtz, mus	1.4-1.5	6.3	Flot
Bernic Lake, Canada	Spodumene, amblygonite, tantalite	Alb, qtz	3.22	7.25	DMS/S.C./Flot/M.S.
Bikita, Zimbabwe	Petalite, lepidolite, amblygonite, eucryptite	n.d.	4.2	4.5-7.3	DMS
Bald Hill, Australia	Spodumene, tantalite	Mus	1.18	6.5	DMS
CBL, Brazil	Spodumene	n.d.	1.4	5.0	DMS
AMG, Brazil	Spodumene, cassiterite, tantalite	Alb, qtz, mus	1.01	5.5	Flot/M.S.

*Alb = Albite, qtz = quartz, mus = muscovite, tur = tourmaline, Flot = flotation, M.S. = magnetic separation, S. C. = spiral circuit, DMS = dense media separation; S.T = shaking table; n.d. – information not described

Figure 4 - Greenbushes spodumene processing flowsheet (modified from BALE; MAY, 1989; GIBSON; AGHAMIRIAN; GRAMMATIKOPOULOS, 2017).



2.6 Process Mineralogy of lithium

The use of automated mineralogy systems in process mineralogy studies improves mineralogical data statistics, thus conferring reliability to the industry in predicting the response of ore reserves to metallurgical treat options (HENLEY, 1986; LOTTER, 1995, 2011). However, SEM-based instruments cannot detect lithium due to limitations of the EDS technique. This results in loss of valuable information such as lithium department and it also limits the use of bulk geochemical analyses even when the mineralogy of the deposit is well known (GRAMMATIKOPOULOS et al., 2021).

Many pegmatite deposits contain both spodumene and lithium-micas in association. The presence of micas in the concentrate results in financial penalty because it increases operational complexity due to problems in the initial calcination stage. It is stated that a spodumene pegmatite deposit where lithium is present at >10% in the minority phases (e.g., micas) is more economically challenging because of the lower “real”¹ head grade once the micas are eliminated (J. WELHAM, 2019). To avoid such issues, it is essential to know the mineral chemistry of all lithium-bearing minerals and determine lithium department. For this, automated mineralogy can be coupled with XRD and mineral chemistry equipment capable of detecting lithium, such as: LA-ICPMS, Time-of-Flight Secondary Ion Mass Spectrometry (ToF-SIMS) and Electron probe micro-analysis (EPMA) (GRAMMATIKOPOULOS et al., 2021).

Two recent examples of process mineralogy studies performed in lithium pegmatite ores in Canada and Australia are presented below and will be used to discuss the results of this work.

Researchers from Canada, performed a study in one sample prepared by compositing three pegmatite zones within one dyke of the Zoro pegmatite lithium project in east-central Manitoba, Canada (GRAMMATIKOPOULOS et al., 2021). For mineralogical analysis samples were crushed to P₈₀ of 600 µm and then screened into four size fractions +600 µm, -600+300 µm, -300+106 µm and -106 µm. Automated mineralogy was used to assess mineral assemblage, liberation of spodumene and potential recovery of spodumene by flotation. Also, heavy liquid separation was

¹ The author mean “real” grade as the lithium content from spodumene.

performed in the coarser size fraction (-6.5 mm + 600 μm) using eight densities from 2.65 to 3.10 to assess the amenability of the sample to DMS to obtain an economically viable lithium concentrate (~6% Li_2O). XRD and SEM-based image analysis (QEMSCAN system) results show that the sample consists of spodumene (10.5%), quartz (29.3%), plagioclase (29.0%), K-feldspar (21.3%), micas (5.1%), tourmaline (2.9%) and Fe-Mn-phosphates (0.1%). Spodumene grains are well-liberated (88%) and accounts for 96% of the total lithium department, while micas account for 2%, Li-Phosphates for 1% and tourmaline and K-feldspar for 1%. Therefore, lithium losses caused by other lithium-bearing minerals are minimal and on considering the high liberation degree of spodumene, flotation can be conducted with ease in relatively coarse particle size ($P_{80} = 600 \mu\text{m}$) to recover spodumene. Feldspar and micas carry considerable amounts of Cs and Rb and could be potential economic sources (AYLMORE et al., 2018b).

The heavy liquid separation results showed that the obtained concentrate had relatively low grade, 5.42 wt% Li_2O , which is less than the target of 6% Li_2O for a commercial concentrate. The Fe_2O_3 content was of 3.7 wt%, which is considered high. The low lithium grade is attributed to the presence of large amounts of iron-silicate minerals reporting to the spodumene concentrate. For further upgrade the concentrate, a dry magnetic belt separator operating at intensity of about 8000 G was used to reject iron-silicate minerals. After the magnetic separation, the concentrate achieved the grade of 6.04 wt% Li_2O , with recovery of 38.1%. Considering that for a given lithium DMS concentrate grade the lithium recovery should be at least in the range of 30 to 50%, results indicate that the ore sample is amenable to beneficiation by DMS operation (GRAMMATIKOPOULOS et al., 2021).

Researchers from Australia used a combination of SEM-based automated mineralogy (TIMA) with ToF-SIMS and LA-ICPMS to characterize samples taken from pegmatite outcrops within Pilbara Minerals Ltd Pilangoora project (AYLMORE et al., 2018b). The samples were combined and subdivided into three subsamples based on their color and texture. The samples were crushed to pass a 3.5 cm screen size and then subjected to electrodynamic fragmentation and screened to pass a 4 mm sieve. Bulk samples were submitted to mineralogical and chemical evaluation and subsamples were screened to produce nine size fractions for mineral liberation studies.

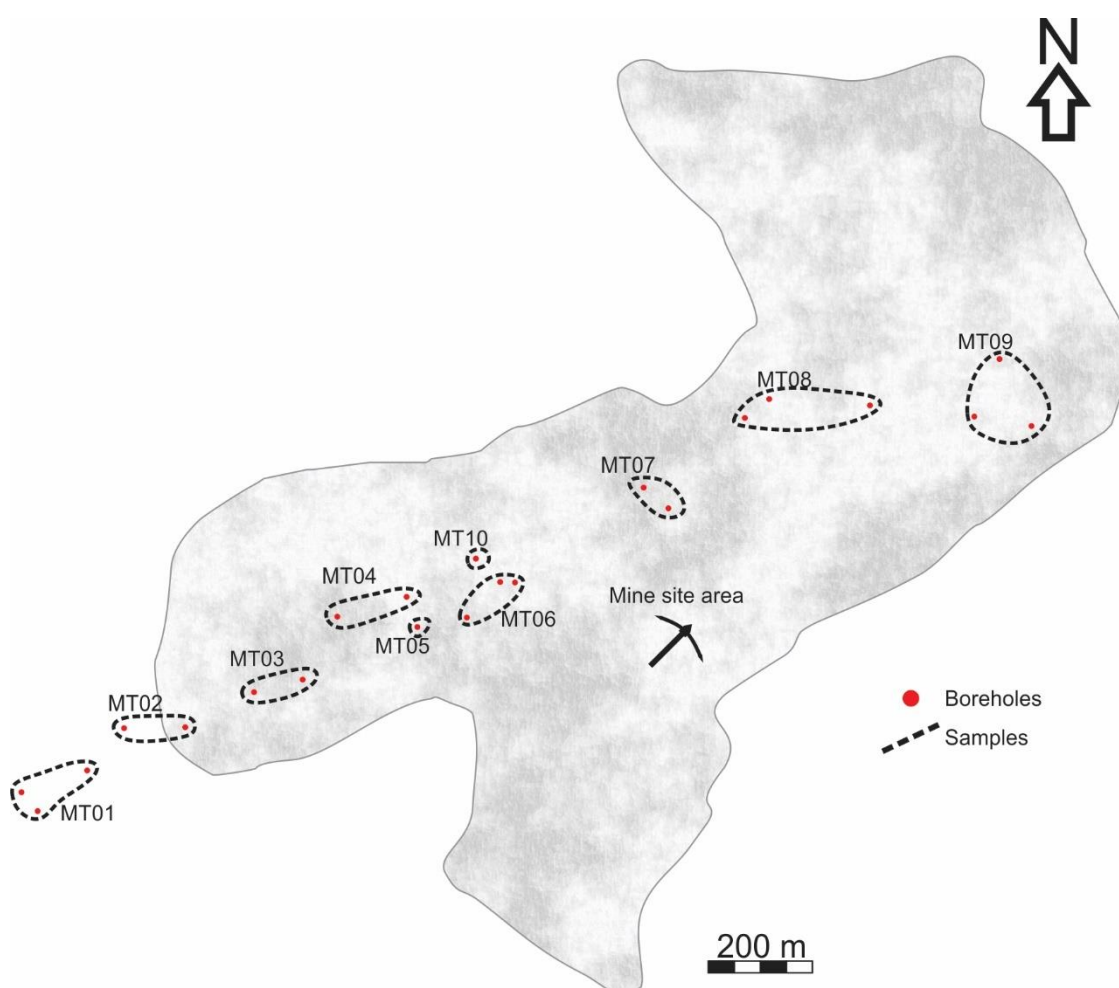
The mineralogical composition obtained by TIMA and XRD shows that all samples are composed of mainly spodumene (~40%), quartz (~30%), feldspar (20-30%), muscovite (~4%), lepidolite (0-5%) and polyolithionite (~0.2%). At P₁₀₀ 4 mm spodumene liberation degree (based on the surface area of spodumene) is between 70 and 90%. The majority of the main gangue minerals can be rejected at coarse grid size (4 mm) to recover 90% of spodumene upgrading the concentrate from 2.1-3.2 wt% Li₂O to 6.5-7.5 wt% Li₂O. The upgrade of spodumene can be achieved by either or a combination of DMS and flotation. Most of the lithium is associated with spodumene (>95%), only a small amount is associated with micas, therefore lithium losses are minimal. High concentration of Rb (0.9-3.6 wt%) and Cs (0.1-0.8 wt%) in feldspar and beryl, respectively, make them a possible resource for these elements.

Further process mineralogy studies performed in lithium micas can be found in literature (AYLMORE et al., 2018a; SANDMANN; GUTZMER, 2013).

3 MATERIALS AND METHODS

Ten samples representing a geographical variation along a lithium enriched pegmatite vein from southern Minas Gerais (Brazil) are the object of this study. Samples were provided by a company whose name and exact location were not allowed to be disclosed. Samples are made up of material of one or up to three boreholes combined (Figure 5). Sampling was carried out by the company's technical personnel, and the samples were sent to the Technological Characterization Laboratory of the University of São Paulo where they were prepared and analyzed.

Figure 5 - Mine site map showing the relative geographic location of the boreholes and samples.



3.1 Broad ore characterization

- The samples arrived in bags with 30 kg of material already grinded at approximately $P_{100} = 4$ mm. In the laboratory, samples were first grinded below $P_{100} = 2$ mm in a rod mill and then divided into twelve subsamples of around 2.5 kg each. One subsample of each sample was used to perform the experimental procedure.

Figure 6A shows the flowsheet of the experimental procedure adopted for the ore characterization study, the steps comprised:

- Visual texture analysis to define a comminution size based on the spodumene average grain size;
- Grinding of each subsample under 0.30 mm in a rod mill and wet screening with screen apertures of 0.30 and 0.037 mm;
- Chemical analyses of bulk sample (-0.30 mm) and all size fractions (-0.30 + 0.037 and -0.037 mm) by X-ray fluorescence (XRF) and inductively coupled plasma optical emission spectroscopy (ICP-OES);
- Mineralogical studies in fraction 0.30-0.037 mm by SEM-based automated mineralogy (SEM-MLA) supported by X-ray diffraction (XRD) to assess minerals composition and spodumene locking and liberation characteristics.
- Mineral heavy liquid separation (fraction 0.30-0.037 mm) using bromoform (s.g. = 2.8) and tetrabromoethane (s.g. = 2.95) for obtaining the following products: float (s.g. < 2.8), intermediate (2.8 < s.g. < 2.95) and sink (s.g. > 2.95), the latter representing spodumene concentrate. All products were sent to chemical analysis (XRF, ICP-OES);

The broad ore characterization study served as a guide to combine similar samples and perform a more detailed process mineralogy study by size fraction on a smaller number of samples.

3.2 Combined samples

- Samples were combined in two groups based on the results of the broad ore characterization study, considering mineralogical and chemical composition,

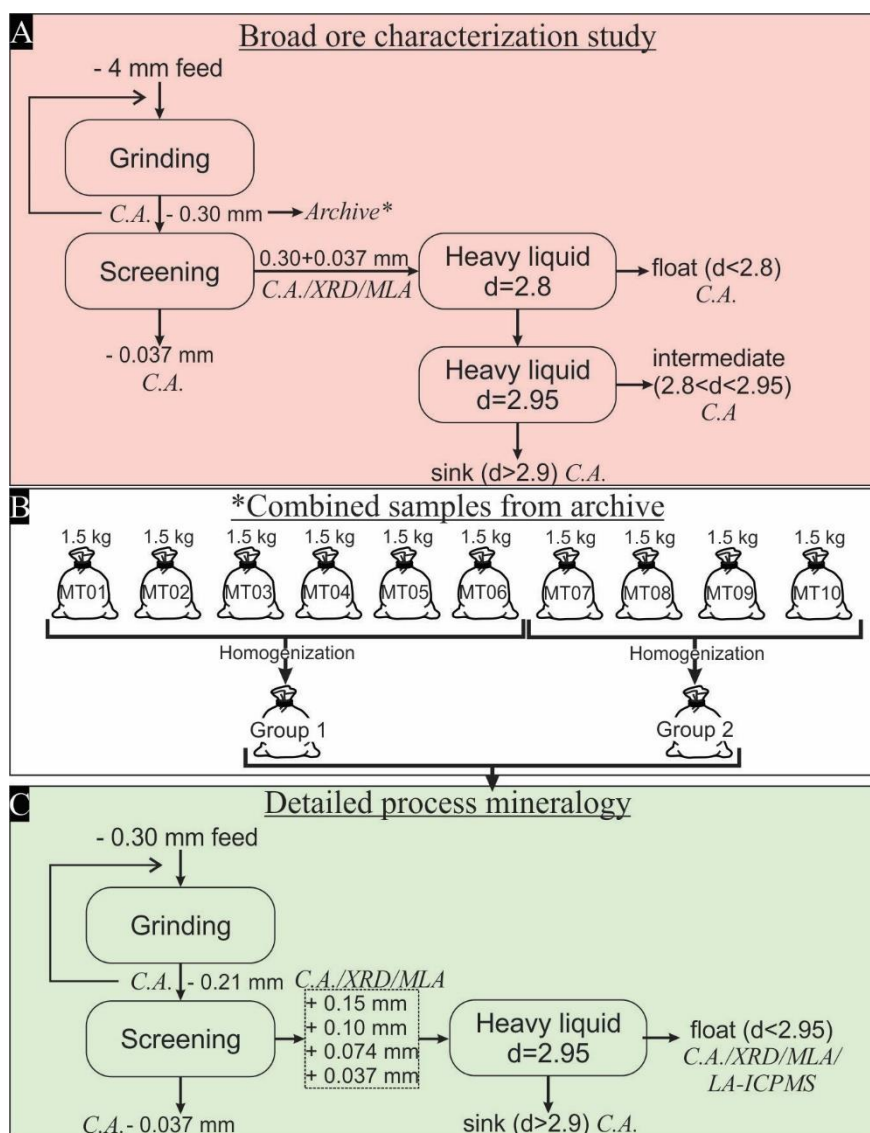
heavy liquid separation results, geographic location and then grouped in Group 1 (G1) and Group 2 (G2) Detailed process mineralogy (Figure 6B).

- Selected grains of lithium-bearing minerals from the float product of the coarser fraction (+0.15 mm) were evaluated by LA-ICPMS to assess their lithium content and determine lithium deportment by heavy liquid separation products

Figure 6C shows the flowsheet of the experimental procedure adopted for the detailed process mineralogy studies performed in the combined samples, the steps comprised:

- Grounding below 0.21 mm in a rod mill (based on broad characterization SEM spodumene liberation observation);
- Wet screening with screen apertures of 0.21, 0.15, 0.10, 0.074, 0.037 mm;
- Chemical analysis were conducted in all fraction sizes and following heavy liquid separation products;
- Detailed mineralogical studies using SEM-based automated mineralogy (MLA) with XRD support were conducted in all fractions over 0.037 mm;
- Heavy liquid separation using tetrabromoethane (s.g. = 2.95) was performed to assess the spodumene concentrate in terms of lithium content and recovery. Also, understand the effect of other lithium-bearing minerals in the test;
- Detailed mineralogical studies using MLA have been performed in the float product (s.g. < 2.95);
- Selected grains of lithium-bearing minerals from the float product of the coarser fraction (+0.15 mm) were evaluated by LA-ICPMS to assess their lithium content and determine lithium deportment by heavy liquid separation products;

Figure 6 - Flowsheet of the experimental procedure of the broad mineral characterization.



3.3 Analytical techniques

XRF, ICP-OES, XRD and SEM analyses were carried out by the Multiuser Centre of the Technological Characterization Laboratory of the University of São Paulo (LCT-USP). LA-ICPMS analysis was performed at the the NAP Geoanalítica-USP (University of São Paulo, Geosciences Institute, Geoanalytical Research Support Center).

3.3.1 Chemical Analysis

Quantitative chemical analyses to determine major elements (Si, Fe, Al, Ca, Mg, Na and K) were undertaken by XRF (Zetium, Panalytical) using fused pellets with

anhydrous lithium tetraborate comparing with certified reference material (AMIS 0355). Qualitative analyses using a standardless procedure were performed to obtain F and Rb contents. Loss on ignition was determined through gravimetry at 1020°C for 2 hours. The lithium content was assessed by ICP-OES (Horiba Ultimate Expert) using samples prepared by fusion with sodium tetraborate.

3.3.2 XRD

Mineralogical analyses were performed by XRD using the powder method in a Bruker D8 Endeavor diffractometer (Co K α , step 0.02°, 38s/step, scanning from 2 to 70°2 θ). The mineral identification was carried out with the software X'Pert Highscore Plus (Panalytical) comparing the diffractograms with the PDF2 dataset of the ICDD (International Centre for Diffraction Data).

3.3.3 SEM based automated mineralogy

Polished section mounts of the size fractions were made to determine the relationship of gangue minerals to spodumene using SEM-based automated image analysis system (MLA software, FEI) (FANDRICH et al., 2007) coupled with SEM-EDS (Quanta 650 FEI, Esprit Bruker Nano Analytics) system.

To perform the automated analysis with MLA the GXMAP measurement mode was used. GXMAP uses X-ray mapping in phases that could not be segmented by backscattering image (BSE) gray levels solely and employs faster area X-ray analysis for phases that are readily segmented (FANDRICH et al., 2007). To well differentiate minerals with similar atomic number (e.g. quartz and plagioclase), contrast was set high, allowing MLA to easily identify several gray levels and then separate them by their chemical composition (characteristic X-ray spectra) by EDS. The X-ray mapping trigger was set to minerals with gray level over 250. Table 4 shows the measurement configuration used.

Table 4 - MLA measurement procedure.

Fractions (mm)	-0.30+0.037	-0.21+0.15	-0.15+0.10	-0.10+0.074	-0.074+0.037
Measurement mode	GXMAP	GXMAP	GXMAP	GXMAP	GXMAP
Number of mounts	1	1	1	1	1
Magnification	150x	150x	200x	250x	250x
Resolution (px)	1000	1000	800	800	800
Pixel size (µm)	1.8	1.8	1.7	1.3	1.3
Frame Overlap X (px)	-	-	-500	-1000	-1000
Frame Overlap Y (px)	-	-	-500	-1000	-1000
Number of particles	~17000	~9000	~9000	~8000	~10000
Main minerals	Quartz	Plagioclase	Spodumene	Muscovite	Lepidolite
Gray levels	~60	~65	~54	~85	~100

Chemical composition and characteristic X-ray of each mineral were inputted at MLA's database, therefore, several mineral grains were chemically analyzed using LEO Stereoscan 440 SEM with EDS detector (INCA x-act. Oxford) calibrated with certified reference standards.

The modal mineral content (in mass) of a phase is calculated by MLA based on area% in the polished section mounts using the density for each mineral. The reliability of the data calculated by MLA were compared with the values obtained by chemical analysis and an R2 value was presented for the major elements of each sample. Some variations in the R2 value are due to variations that were not modelled in mineral compositions, such as lithium, iron, sodium, potassium, silica, and aluminum contents in micas.

3.3.4 LA-ICPMS

Lithium is not detected using standard energy dispersive X-ray spectrometers mounted on electron microscopes due to its characteristic low energy X-rays. Therefore, the quantification of lithium in some minerals was assessed by LA-ICPMS, using a New Wave UP-213A/F 213 nm laser coupled with a Perkin Elan-6100DRC quadrupole ICPMS (30 µm diameter spot, frequency 15 Hz, fluence of 1.13 j/cm², 30s ablation, and 15s baseline) operating in a He+Ar atmosphere. Grain composition were determined using NIST610 standard and stoichiometry standardized using Si for each mineral derived from data of EDS analyses.

4 RESULTS

4.1 Broad ore characterization

4.1.1 Bulk chemical analysis

The chemical composition of the samples is shown in Table 5. Samples MT01, MT02, MT03, MT04, and MT06 have average Li₂O content of 1.44 wt%, while MT05, MT07, MT08, MT09, and MT10 average content is 0.65 wt%. The Fe₂O₃ content ranges between 0.20 to 0.80 wt% in samples MT01 to MT09, while sample MT10 has 1.10 wt%. CaO content ranges between 0.30 to 0.63 wt% in samples MT01 to MT09, while sample MT10 has 1.30 wt%. The Rb₂O content ranges between 0.91 and 0.32 wt% in samples MT02 to MT10, while sample MT01 has 1.14 wt%. Contents of SiO₂, Al₂O₃, Na₂O, K₂O, and MnO are quite similar in all samples, averaging ~ 73.0, ~ 15.5, ~ 43.5, ~ 2.00, ~ 0.15 wt%, respectively. F content is generally lower than the detection limit (<0.001 wt%), except in samples MT01, MT02, MT03, and MT04 in which the average F content is 0.78 wt%.

Table 5 - Bulk chemical analysis.

Element	LiO ₂	SiO ₂	Fe ₂ O ₃	Al ₂ O ₃	CaO	MgO	Na ₂ O	K ₂ O	F	Rb ₂ O	Total
MT01	1.08	70.5	0.28	16.9	0.36	<0.01	4.52	2.66	1.03	1.14	100
MT02	1.45	74.5	0.20	15.1	0.30	<0.01	3.94	1.63	0.71	0.84	100
MT03	1.74	71.1	0.43	17.0	0.63	<0.01	3.55	1.78	0.92	0.91	99.9
MT04	1.43	73.5	0.28	15.5	0.32	<0.01	4.11	1.68	0.44	0.65	99.8
MT05	0.25	71.9	0.51	16.2	0.31	<0.01	4.42	1.23	-	0.32	98.3
MT06	1.51	73.4	0.45	15.5	0.34	<0.01	3.62	1.85	-	0.66	98.9
MT07	0.93	74.3	0.65	15.0	0.64	<0.01	4.72	1.64	-	0.49	99.9
MT08	0.75	71.7	0.65	16.2	0.46	<0.01	5.11	1.90	-	0.44	100
MT09	0.75	73.7	0.81	15.6	0.63	0.36	4.91	1.71	-	0.50	100
MT10	0.58	73.6	1.10	13.4	1.30	0.34	4.68	1.14	-	0.37	98.0

4.1.2 Assessment of mineral content

The mineralogical composition of samples in fraction -0.30 +0.037 mm is shown in Table 6. In general, samples are made up of quartz (~40%), albite (~34%) and mica (~16%). Samples MT02, MT03, MT04 and MT06 have a higher spodumene content

(13 – 19%), reaching up to twice as much as in the other samples (3 – 9%). Sample MT01 has almost twice as much mica (27%) than all other samples (11 – 20%).

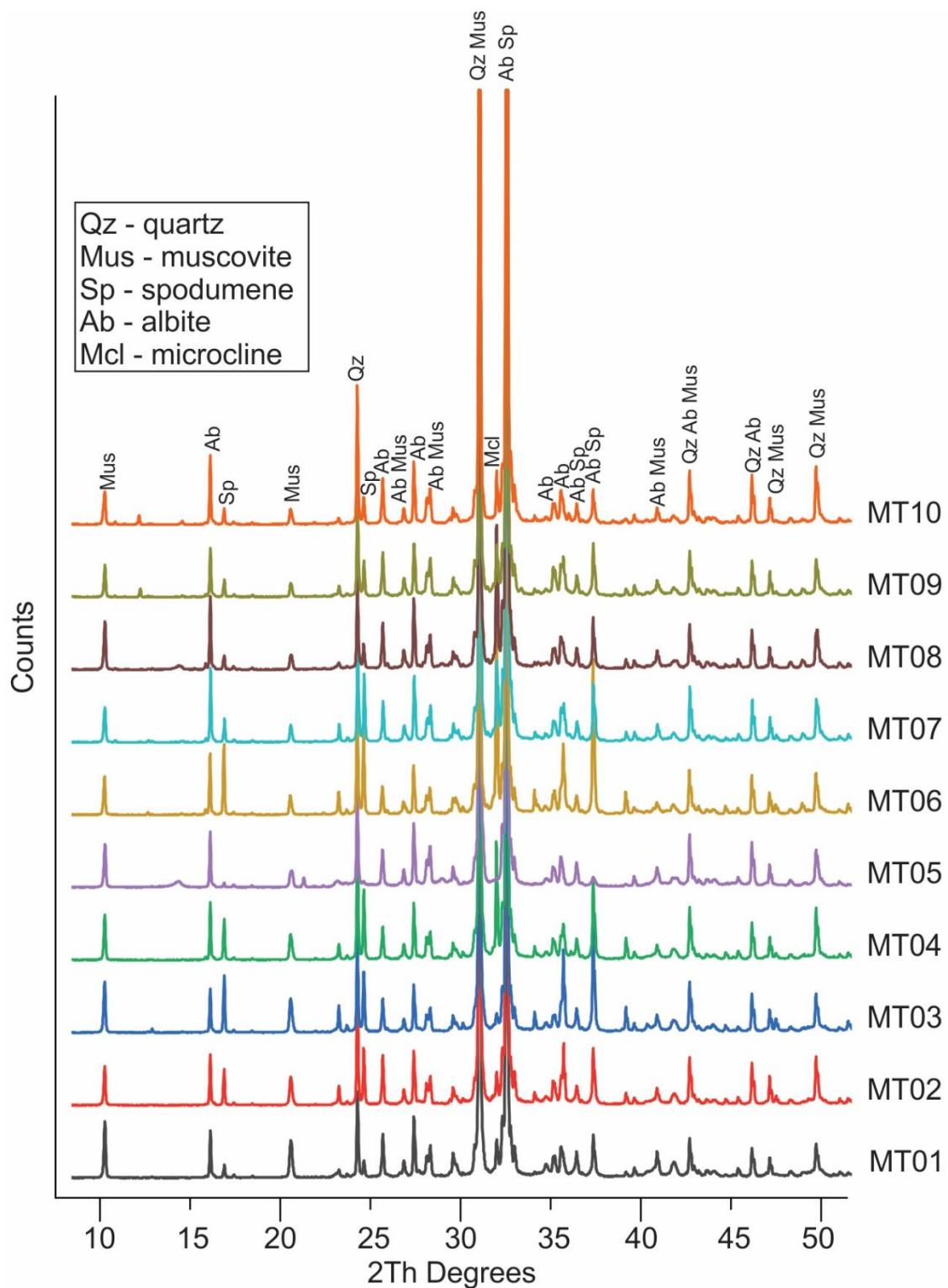
Table 6 – MLA calculated mineralogical composition of the -0.30+0.037 mm size fraction.

Mineral	MT01	MT02	MT03	MT04	MT05	MT06	MT07	MT08	MT09	MT10
quartz	30	38	31	35	40	34	34	32	33	40
albite	34	29	27	29	40	28	38	40	40	38
mica	27	19	20	16	14	16	13	16	14	11
spodumene	6.8	13	19	18	2.9	19	10	6.9	9.1	5.0
K-feldspar	0.8	0.4	0.4	0.9	0.2	1.8	1.8	2.8	1.9	0.9
epidote	0.3	0.2	2.1	0.3	0.3	0.7	1.8	1.2	0.9	4.7
garnet	0.1	0.0	0.0	0.1	0.1	0.1	0.2	0.2	1.0	0.7
apatite	0.2	0.1	0.3	0.2	0.1	0.2	0.3	0.1	0.2	0.3
cassiterite	0.23	0.02	0.02	0.01	0.01	0.03	0.06	0.04	0.07	0.05
kaolinite	0.01	0.02	0.05	0.02	2.24	0.01	0.01	0.44	0.01	0.00
microlite	0.06	0.18	0.20	0.08	0.03	0.03	0.07	0.05	0.06	0.05
columbite	0.01	0.00	0.13	0.01	0.06	0.01	0.02	0.02	0.04	0.02
others*	0.30	0.18	0.13	0.10	0.22	0.17	0.09	0.07	0.05	0.10

*others: sphalerite, gibbsite, fluorite, amphibole, barite

Figure 7 shows the bulk sample XRD data, all samples are made up of predominantly quartz, albite, muscovite, spodumene and microcline. Samples MT02, MT03, MT04, and MT06 have higher spodumene line intensities than the other samples. Samples MT04, MT06, MT07, and MT08 have higher microcline line intensities than the other samples. XRD cannot distinguish accurately between the different lithium-bearing micas, therefore, the muscovite identified represents a combination of different micas.

Figure 7 – Bulk sample XRD patterns.



4.1.3 Sieve analysis

Table 7 shows the results of the screening test in terms of mass distribution, content of the major elements present, and the distribution percentage of each element

between size fractions. In general, around 75% of the mass reports to fraction 0.30 + 0.037 mm while 25% reports to fraction -0.037 mm.

In fraction -0.30 + 0.037 mm, Li₂O average content in samples MT01, MT02, MT03, MT04, and MT06 is 1.56 wt%. Samples MT05, MT07, MT08, MT09, and MT10 average Li₂O content is 0.62 wt%. The deportment of lithium in this fraction is ~ 75% in all samples. Content of SiO₂ (~ 75.3 wt%), Al₂O₃ (~ 17.4 wt%), K₂O (~ 1.79 wt%), Fe₂O₃ (~ 0.45 wt%), and CaO (~ 0.44 wt%) do not vary much between samples. The deportment of Fe₂O₃ is ~ 64% and of CaO is ~ 59%. The deportment of SiO₂ and Al₂O₃ is ~ 76% and ~ 72%, respectively, and the K₂O deportment is ~ 76%.

In fraction -0.037 mm, average Li₂O content in samples MT01, MT02, MT03, MT04, and MT06 is 1.22 wt%. Samples MT05, MT07, MT08, MT09, and MT10 have average Li₂O content of 0.57 wt%. The deportment of lithium in this fraction is ~ 25% in all samples.

4.1.4 Spodumene characteristics

Figure 8 shows the general mineral composition of each sample in the polished mounts of fraction -0.30 + 0.037 mm. Samples MT01, MT02, MT03, MT04, and MT06 are more abundant in well liberated coarse spodumene grains, which often present tabular shape. The main gangue minerals are plagioclase, quartz, and mica (Figure 8a, b, c, d, f). Samples MT05, MT 07, MT 08, MT09, and MT10 have less and generally smaller spodumene grains. The main gangue minerals are plagioclase and quartz (Figure 8e, g, h, i, j).

Figure 9 shows the size distribution of spodumene grains for all samples considering an equivalent circle diameter (ECD) of the particles. Samples MT01, MT02, MT03, MT04, and MT06 have spodumene grains with an average size of approximately 100 µm, while samples MT05, MT07, MT08, MT09, and MT10 have spodumene grains with an average size of approximately 60 µm.

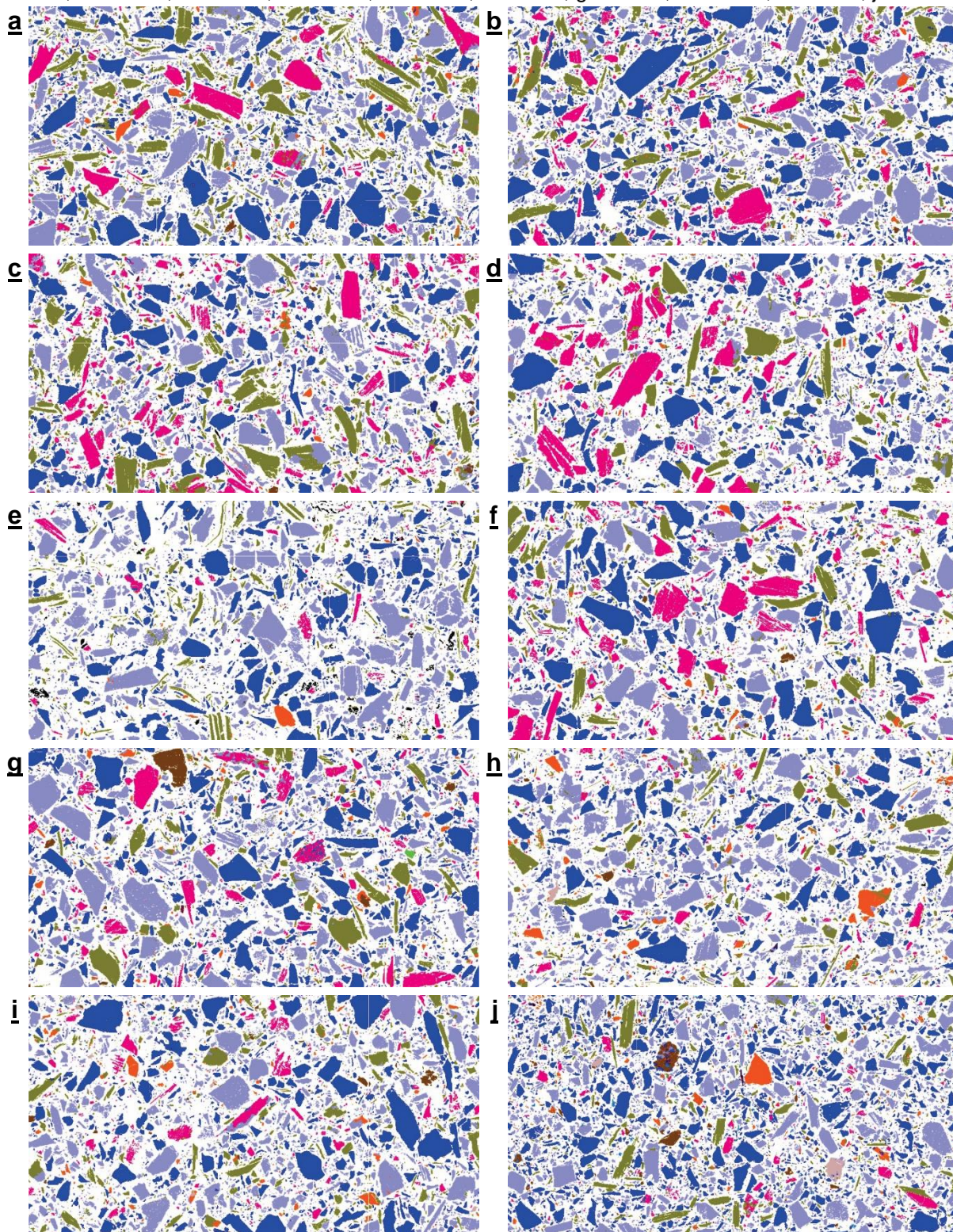
Table 7 - Chemical analysis by size fraction of the ten samples.

AM	Size fraction (mm)	Mass retained (%)	Content (wt%)							Department in test (%)						
			Li ₂ O	Fe ₂ O ₃	SiO ₂	Al ₂ O ₃	CaO	K ₂ O	LOI	Li ₂ O	Fe ₂ O ₃	SiO ₂	Al ₂ O ₃	CaO	K ₂ O	LOI
MT01	-0.30+0.037	76.0	1.01	0.26	70.1	16.9	0.24	2.77	2.05	81.3	68.2	75.8	76.7	49.4	79.0	83.0
	-0.037	24.0	0.74	0.39	71.0	16.3	0.78	2.33	1.33	18.8	31.8	24.2	23.3	50.6	21.0	17.0
	Total calculated	100.0	0.95	0.29	70.3	16.8	0.37	2.66	1.88	100.0	100.0	100.0	100.0	100.0	100.0	100.0
	Chemical analysis		1.06	0.28	70.5	16.9	0.36	2.66	2.14							
MT02	-0.30+0.037	74.6	1.50	0.16	74.7	15.1	0.18	1.68	1.30	79.3	64.8	74.4	75.1	46.9	78.4	81.8
	-0.037	25.4	1.15	0.25	75.5	14.6	0.61	1.35	0.85	20.7	35.2	25.6	24.8	53.1	21.5	18.2
	Total calculated.	100.0	1.41	0.18	74.9	14.9	0.29	1.59	1.19	100.0	100.0	100.0	100.0	100.0	100.0	100.0
	Chemical analysis		1.39	0.20	74.5	15.1	0.30	1.63	1.59							
MT03	-0.30+0.037	77.5	1.97	0.32	71.3	16.6	0.54	1.79	1.64	79.7	59.4	77.7	77.1	65.1	79.2	85.2
	-0.037	22.5	1.72	0.75	70.7	17.1	0.99	1.63	0.98	20.3	40.7	22.3	23.0	34.9	20.9	14.8
	Total calculated.	100.0	1.91	0.41	71.2	16.8	0.64	1.76	1.49	100.0	100.0	100.0	100.0	100.0	100.0	100.0
	Chemical analysis		1.92	0.43	71.1	17.0	0.63	1.78	1.82							
MT04	-0.30+0.037	73.1	1.64	0.39	75.6	14.8	0.26	1.85	1.08	79.1	72.5	73.7	71.7	56.7	74.8	78.1
	-0.037	26.9	1.18	0.40	73.4	15.9	0.54	1.69	0.82	20.9	27.5	26.3	28.3	43.3	25.1	21.9
	Total calculated.	100.0	1.52	0.39	75.0	15.1	0.34	1.81	1.01	100.0	100.0	100.0	100.0	100.0	100.0	100.0
	Chemical analysis		1.43	0.28	73.5	15.5	0.32	1.68	1.38							
MT05	-0.30+0.037	74.3	0.28	0.47	77.4	13.7	0.26	1.35	1.84	79.0	67.5	77.4	64.9	58.5	78.8	55.2
	-0.037	25.7	0.21	0.66	65.3	21.4	0.54	1.05	4.31	21.0	32.5	22.6	35.1	41.5	21.2	44.8
	Total calculated	100.0	0.26	0.52	74.3	15.7	0.33	1.27	2.48	100	100	100	100	100	100	100
	Chemical analysis		0.25	0.51	71.9	16.2	0.31	1.23	3.16							

Table 7 – Continuation of the chemical analysis by size fraction of the ten samples

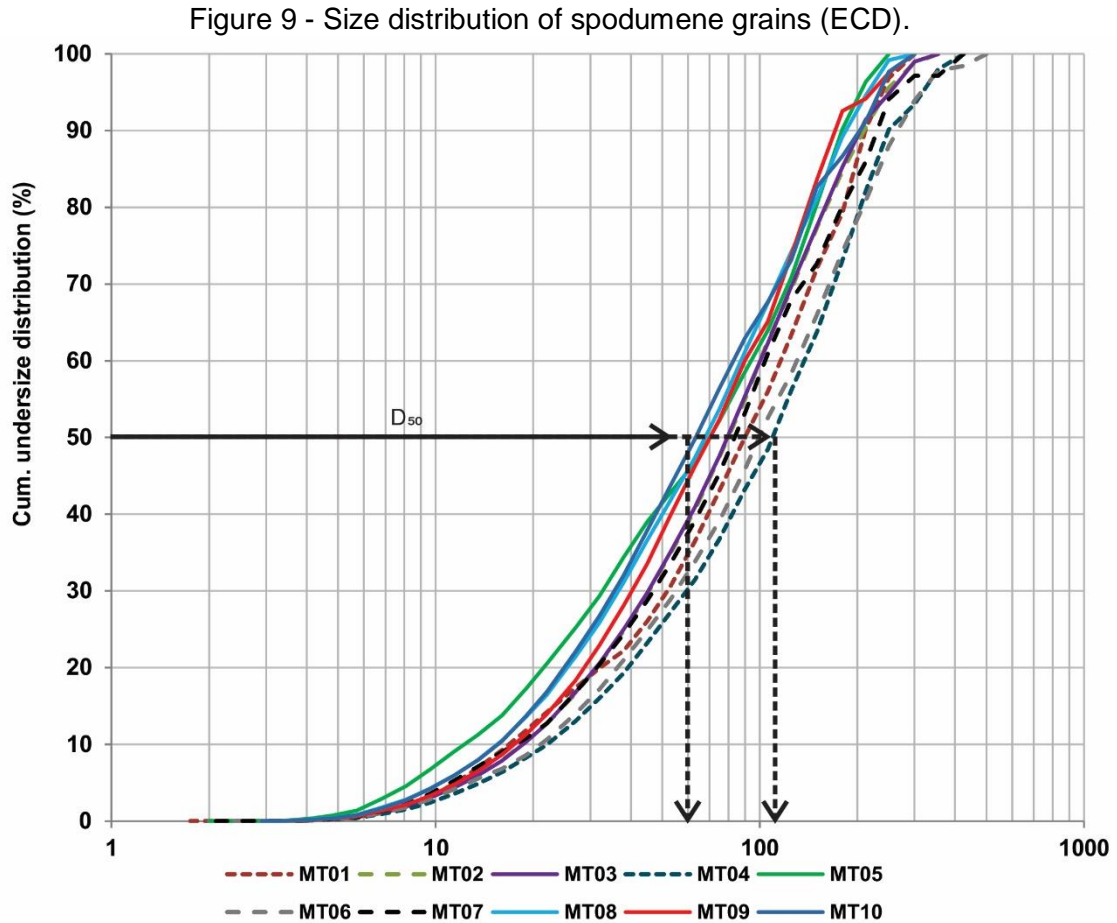
	Size Fraction (mm)	Mass retained (%)	Content (wt%)							Department in test (%)						
			Li ₂ O	Fe ₂ O ₃	SiO ₂	Al ₂ O ₃	CaO	K ₂ O	LOI	Li ₂ O	Fe ₂ O ₃	SiO ₂	Al ₂ O ₃	CaO	K ₂ O	LOI
MT06	-0.30+0.037	77.3	1.68	0.38	76.9	14.7	0.31	1.92	0.94	81.5	63.6	78.2	75.8	63.6	76.0	77.2
	-0.037	22.7	1.30	0.74	72.8	16.0	0.61	2.06	0.94	18.5	36.3	21.8	24.2	36.4	23.9	22.7
	Total calculated	100.0	1.60	0.46	75.9	15.0	0.38	1.95	0.94	100.0	100.0	100.0	100.0	100.0	100.0	100.0
	Chemical analysis		1.51	0.45	73.4	15.5	0.34	1.85	1.23							
MT07	-0.30+0.037	78.1	0.84	0.53	76.9	13.8	0.56	1.63	0.93	75.7	62.4	79.2	75.2	67.5	76.4	82.2
	-0.037	21.9	0.96	1.13	71.8	16.2	0.96	1.79	0.72	24.3	37.6	20.8	24.8	32.5	23.6	17.8
	Total calculated	100.0	0.86	0.66	75.8	14.3	0.65	1.66	0.89	100.0	100.0	100.0	100.0	100.0	100.0	100.0
	Chemical analysis		0.89	0.65	74.3	15.0	0.64	1.64	1.16							
MT08	-0.30+0.037	77.1	0.68	0.59	75.7	14.6	0.37	2.05	1.16	80.3	69.1	78.6	73.2	65.6	78.9	66.9
	-0.037	22.9	0.56	0.89	69.5	18.0	0.66	1.85	1.93	19.7	31.0	21.4	26.8	34.4	21.1	33.1
	Total calculated	100.0	0.66	0.66	74.3	15.4	0.44	2.00	1.33	100.0	100.0	100.0	100.0	100.0	100.0	100.0
	Chemical analysis		0.66	0.65	71.7	16.2	0.46	1.90	1.78							
MT09	-0.30+0.037	74.0	0.77	0.55	76.5	14.5	0.52	1.62	0.94	75.9	57.5	75.4	71.5	61.5	71.8	74.0
	-0.037	26.0	0.69	1.15	70.8	16.4	0.93	1.81	0.94	24.1	42.5	24.5	28.4	38.5	28.2	26.0
	Total calculated	100.0	0.75	0.70	75.0	15.0	0.63	1.67	0.94	100.0	100.0	100.0	100.0	100.0	100.0	100.0
	Chemical analysis		0.80	0.81	73.7	15.6	0.63	1.71	1.24							
MT10	-0.30+0.037	68.1	0.53	0.83	77.5	12.6	1.14	1.19	0.95	72.6	51.9	69.5	64.8	58.3	68.7	70.3
	-0.037	31.9	0.42	1.63	72.5	14.6	1.73	1.16	0.85	27.4	48.0	30.5	35.1	41.6	31.3	29.6
	Total calculated	100.0	0.49	1.08	75.9	13.3	1.33	1.18	0.92	100.0	100.0	100.0	100.0	100.0	100.0	100.0
	Chemical analysis		0.52	1.10	73.6	13.4	1.30	1.14	1.25							

Figure 8 - MLA mineral composition maps in the $-0.30 + 0.037$ mm size fraction for all ten samples: a – MT01, b – MT02, c – MT03, d – MT04, e – MT05, f – MT06, g – MT07, h – MT08, i – MT09, j – MT10.



500 μm





4.1.5 Mineral heavy liquid separation

Table 8 shows the heavy liquid separation test results performed in fraction - 0.30 + 0.037 mm. In all samples the floated and middling products account together for ~ 90% in mass of the test (65% in mass of the samples), while the sunken products account for ~ 10% in mass of the test (7.5% of the samples).

The Li_2O content is generally two or three times higher in the sunken products than in the middling products ranging from ~ 4.0 wt% (MT10) to 7.4 wt% (MT02, MT04, MT06). The lowest Li_2O content is registered in the floated product, ranging from ~ 0.1 wt% (MT05, MT07, MT08, MT09, MT10) to 1.0 wt% (MT03, MT06).

The deportment of Li_2O in the sunken product of samples MT01 to MT06 represents ~ 50% of the test (40% of the sample), and in samples MT07 to MT10 ~ 83% of the test (63% of the sample).

Fe_2O_3 content in the sunken product of samples MT01, MT02, MT04, and MT06 averages 0.55 wt%, and in samples MT05, MT07, MT08, MT09, and MT10 averages ~ 2.62 wt%. The Fe_2O_3 deportment in the sunken product of samples MT01, MT02, MT04, MT05, and MT06 is ~ 16% of the test (11% of the sample), and in samples MT03, MT07, MT08, and MT09 ~ 42% of the test (25% in the sample).

The CaO content in the sunken product of samples MT01 to MT06 averages 1.15 wt%, and in samples MT05 to MT10 the content is ~ 4.00%. The CaO deportment in the sunken product of the test ranges between ~ 32% (16% of the sample) and 81% (40% of the sample).

SiO_2 content in the floated products are ~ 80 wt% which accounts for ~ 90% of the SiO_2 deportment of the test (67% of the sample). Al_2O_3 content in the floated products are ~ 80 wt% which accounts for approximately 90% of the SiO_2 deportment in the floated product of the test (67% of the sample).

Al_2O_3 content in the sunken and middling products are similar (~ 25 wt%). The content in the floated product is ~13% and accounts for ~76% of the Al_2O_3 deportment in the test (60% of the sample).

K_2O content in the middling products are ~ 6 wt%. Despite that, the floated products (~ 1.80 wt%) account for ~ 87% of the K_2O deportment in the test (69% of the sample).

Table 8 – Heavy liquid separation results for the -0.30 + 0.037 mm size fraction in all ten samples.

	Fraction (mm)	Product	Mass (%)		Content (wt%)							Department in test (%)							Department in sample (%)						
			Test	Sample	Li ₂ O	Fe ₂ O ₃	SiO ₂	Al ₂ O ₃	CaO	K ₂ O	LOI	Li ₂ O	Fe ₂ O ₃	SiO ₂	Al ₂ O ₃	CaO	K ₂ O	LOI	Li ₂ O	Fe ₂ O ₃	SiO ₂	Al ₂ O ₃	CaO	K ₂ O	LOI
MT01	-0.30+0.037	d<2.80	88.1	67.0	0.58	0.21	71.9	15.7	0.12	2.64	1.96	50.1	70.0	90.3	81.6	43.9	84.0	84.4	40.7	47.8	68.5	62.6	21.7	66.4	70.0
		2.80<d<2.95	5.27	4.01	1.91	0.72	50.6	26.5	0.09	7.73	4.99	9.93	14.4	3.80	8.24	1.97	14.7	12.8	8.07	9.80	2.88	6.32	0.97	11.6	10.6
		d>2.95	6.67	5.07	6.06	0.62	61.5	25.9	1.95	0.54	0.85	39.9	15.7	5.85	10.2	54.1	1.30	2.78	32.4	10.7	4.44	7.82	26.7	1.03	2.30
		Total calc.	100	76.0	1.01	0.26	70.1	16.9	0.24	2.77	2.05	100	100	100	100	100	100	100	81.2	68.2	75.8	76.7	49.4	79.0	83.0
MT02	-0.30+0.037	d<2.80	88.2	65.7	0.89	0.12	76.6	13.6	0.14	1.64	1.23	52.7	67.5	90.4	79.6	67.3	86.3	83.4	41.8	43.7	68.5	61.1	33.3	68.2	69.3
		2.80<d<2.95	3.18	2.37	2.11	0.59	56.2	24.4	0.06	6.56	3.79	4.49	11.98	2.39	5.15	1.04	12.4	9.28	3.56	7.76	1.81	3.96	0.51	9.84	7.70
		d>2.95	8.67	6.46	7.39	0.37	62.5	26.4	0.67	0.25	1.09	42.8	20.5	7.25	15.2	31.7	1.29	7.28	33.9	13.3	5.50	11.7	15.7	1.02	6.04
		Total calc.	100	74.6	1.50	0.16	74.7	15.1	0.18	1.68	1.30	100	100	100	100	100	100	100	79.3	64.8	75.8	76.7	49.4	79.0	83.0
MT03	-0.30+0.037	d<2.80	77.4	60.0	1.02	0.21	74.7	14.2	0.32	1.65	1.55	40.0	51.2	81.0	66.0	46.1	71.1	73.0	31.9	30.4	61.4	50.6	22.8	56.2	60.6
		2.80<d<2.95	7.64	5.92	1.93	0.46	58.4	22.7	0.11	6.19	4.14	7.5	11.1	6.3	10.4	1.57	26.4	19.3	5.96	6.57	4.74	7.99	0.77	20.8	16.0
		d>2.95	15.0	11.63	6.89	0.80	60.5	26.2	1.87	0.30	0.85	52.5	37.8	12.7	23.6	52.3	2.51	7.77	41.9	22.4	9.6	18.1	25.8	1.98	6.45
		Total calc.	100	77.5	1.97	0.32	71.3	16.6	0.54	1.79	1.64	100	100	100	100	100	100	100	79.7	59.4	75.8	76.7	49.4	79.0	83.0
MT04	-0.30+0.037	d<2.80	83.4	60.9	0.88	0.37	78.4	12.8	0.22	1.86	1.05	44.6	79.6	86.4	72.1	70.5	83.8	81.3	35.3	57.7	65.5	55.3	34.9	66.2	67.5
		2.80<d<2.95	4.95	3.62	1.50	0.61	60.8	21.5	0.04	5.53	2.95	4.53	7.79	3.98	7.19	0.76	14.8	13.6	3.58	5.64	3.02	5.52	0.38	11.7	11.3
		d>2.95	11.68	8.54	7.14	0.42	62.2	26.3	0.64	0.23	0.47	50.9	12.7	9.61	20.7	28.7	1.45	5.10	40.2	9.17	7.28	15.9	14.2	1.15	4.23
		Total calc.	100	73.1	1.64	0.39	75.6	14.8	0.26	1.85	1.08	100	100	100	100	100	100	100	79.1	72.5	75.8	76.7	49.4	79.0	83.0
MT05	-0.30+0.037	d<2.80	96.5	71.7	0.09	0.39	78.2	13.3	0.16	1.33	1.84	31.7	79.4	97.6	93.7	58.7	94.9	96.4	25.0	53.6	73.9	71.9	29.0	75.0	80.0
		2.80<d<2.95	0.88	0.65	0.93	2.12	52.7	25.6	0.16	6.59	5.27	2.96	3.94	0.60	1.64	0.53	4.29	2.52	2.34	2.66	0.45	1.26	0.26	3.39	2.09
		d>2.95	2.60	1.93	6.97	3.03	54.6	24.4	4.13	0.42	0.73	65.3	16.6	1.84	4.63	40.8	0.81	1.03	51.6	11.2	1.39	3.55	20.2	0.64	0.86
		Total calc.	100	74.3	0.28	0.47	77.4	13.7	0.26	1.35	1.84	100	100	100	100	100	100	100	79.0	67.5	75.8	76.7	49.4	79.0	83.0

Table 8 - Heavy liquid separation results for the -0.30 + 0.037 mm size fraction in all ten samples.

	Fraction (mm)	Product	Mass (%)		Content (wt%)							Department in test (%)							Department in sample (%)						
			Test	Sample	Li ₂ O	Fe ₂ O ₃	SiO ₂	Al ₂ O ₃	CaO	K ₂ O	LOI	Li ₂ O	Fe ₂ O ₃	SiO ₂	Al ₂ O ₃	CaO	K ₂ O	LOI	Li ₂ O	Fe ₂ O ₃	SiO ₂	Al ₂ O ₃	CaO	K ₂ O	LOI
MT06	-0.30+0.037	d<2.80	84.3	65.1	0.95	0.33	79.7	12.8	0.28	1.98	0.87	47.6	73.1	87.4	73.3	75.3	86.8	78.0	38.8	46.5	66.3	56.2	37.2	68.6	64.8
		2.80<d<2.95	4.13	3.19	1.31	0.97	61.1	21.6	0.08	5.61	2.93	3.21	10.5	3.28	6.06	1.05	12.0	12.9	2.62	6.69	2.49	4.65	0.52	9.52	10.7
		d>2.95	11.6	8.96	7.14	0.54	61.8	26.3	0.64	0.20	0.74	49.2	16.5	9.33	20.7	23.7	1.21	9.12	40.1	10.5	7.07	15.9	11.7	0.95	7.57
		Total calc.	100	77.3	1.68	0.38	76.9	14.7	0.31	1.92	0.94	100	100	100	100	100	100	100	81.5	63.6	75.8	76.8	49.4	79.1	83.0
MT07	-0.30+0.037	d<2.80	86.8	67.8	0.16	0.34	79.8	12.0	0.25	1.69	0.86	16.7	56.2	90.1	75.6	38.8	90.2	79.9	12.6	35.0	68.3	58.0	19.2	71.3	66.3
		2.80<d<2.95	1.93	1.51	1.17	2.61	53.7	25.9	0.26	6.57	3.83	2.68	9.59	1.35	3.63	0.90	7.80	7.92	2.03	5.98	1.02	2.78	0.44	6.16	6.58
		d>2.95	11.3	8.83	5.98	1.59	58.4	25.4	2.99	0.29	1.011	80.6	34.2	8.58	20.8	60.4	2.02	12.2	61.0	21.3	6.51	16.0	29.8	1.59	10.2
		Total calc.	100	78.1	0.84	0.53	76.9	13.8	0.56	1.63	0.93	100	100	100	100	100	100	100	75.7	62.4	75.8	76.8	49.4	79.0	83.0
MT08	-0.30+0.037	d<2.80	89.5	69.0	0.10	0.42	77.9	13.3	0.18	2.12	1.14	13.0	63.8	92.1	81.4	43.1	92.5	88.2	10.4	44.0	69.8	62.5	21.3	73.2	73.2
		2.80<d<2.95	1.51	1.16	1.15	4.50	49.5	27.2	0.21	7.56	4.54	2.53	11.5	0.99	2.81	0.85	5.57	5.93	2.04	7.96	0.75	2.16	0.42	4.40	4.92
		d>2.95	8.99	6.93	6.42	1.62	58.5	25.7	2.33	0.43	0.75	84.5	24.7	6.94	15.8	56.0	1.89	5.83	67.9	17.1	5.26	12.1	27.7	1.49	4.84
		Total calc.	100	77.1	0.68	0.59	75.7	14.6	0.37	2.05	1.16	100	100	100	100	100	100	100	80.3	69.1	75.8	76.7	49.4	79.0	83.0
MT09	-0.30+0.037	d<2.80	86.1	63.7	0.11	0.23	79.6	12.8	0.23	1.71	0.95	12.1	36.2	89.6	76.0	37.9	90.8	86.9	9.2	20.8	67.9	58.4	18.7	71.8	72.1
		2.80<d<2.95	1.78	1.32	1.16	2.70	51.9	27.5	0.54	6.92	3.13	2.68	8.79	1.21	3.38	1.84	7.60	5.92	2.04	5.05	0.92	2.59	0.91	6.01	4.91
		d>2.95	12.1	8.97	5.39	2.48	58.0	24.6	2.6	0.21	0.56	85.2	55.0	9.20	20.6	60.3	1.57	7.22	64.6	31.6	6.97	15.8	29.8	1.24	5.99
		Total calc.	100	74.0	0.77	0.55	76.5	14.5	0.52	1.62	0.94	100	100	100	100	100	100	100	75.9	57.5	75.8	76.7	49.4	79.0	83.0
MT10	-0.30+0.037	d<2.80	87.2	59.4	0.08	0.34	81.0	11.0	0.22	1.22	0.88	14.0	35.9	91.1	76.0	16.9	89.2	81.2	10.2	18.6	69.0	58.3	8.4	70.5	67.4
		2.80<d<2.95	1.84	1.25	1.20	2.72	58.0	23.0	1.14	5.25	3.61	4.18	6.06	1.38	3.35	1.85	8.10	7.01	3.03	3.15	1.04	2.57	0.91	6.40	5.82
		d>2.95	11.0	7.46	3.94	4.37	53.3	23.8	8.42	0.29	1.02	81.8	58.0	7.53	20.7	81.3	2.67	11.8	59.4	30.1	5.71	15.9	40.2	2.11	9.82
		Total calc.	100	68.1	0.53	0.83	77.5	12.6	1.14	1.19	0.95	100	100	100	100	100	100	100	72.6	51.9	75.8	76.7	49.4	79.0	83.0

4.2 Combined samples

For the detailed process mineralogy study, samples were combined into two new samples considering several criteria that will be discussed below.

The criteria considered to combine samples were: lithium content in the bulk sample; spodumene content in fraction $-0.30+0.037$ mm; lithium content and deportment in the heavy liquid separation products; and the relative geographic location of samples.

Samples MT01 to MT06 have higher Li_2O content in the bulk sample and higher spodumene content in fraction $-0.30 + 0.037$ mm (Figure 11 a and b) than samples MT07 to MT10. In the heavy liquid separation test, the sunken product of these samples have lower Li_2O deportment, but a relatively higher Li_2O content (Figure 12) than samples MT07 to MT10. Although sample MT05 does not fit so well with the trends cited above, geographically it made more sense to consider it as part of Group 1 (Figure 10).

On the other hand, samples MT07 to MT10 have a lower Li_2O content in the bulk sample and lower spodumene content in fraction $-0.30 + 0.037$ mm (Figure 11 a and b). In the heavy liquid separation test, the sunken product of these samples presents higher Li_2O deportment and slightly lower Li_2O content (Figure 12).

Figure 10 - Mine site map showing the geographic layout of the groups.

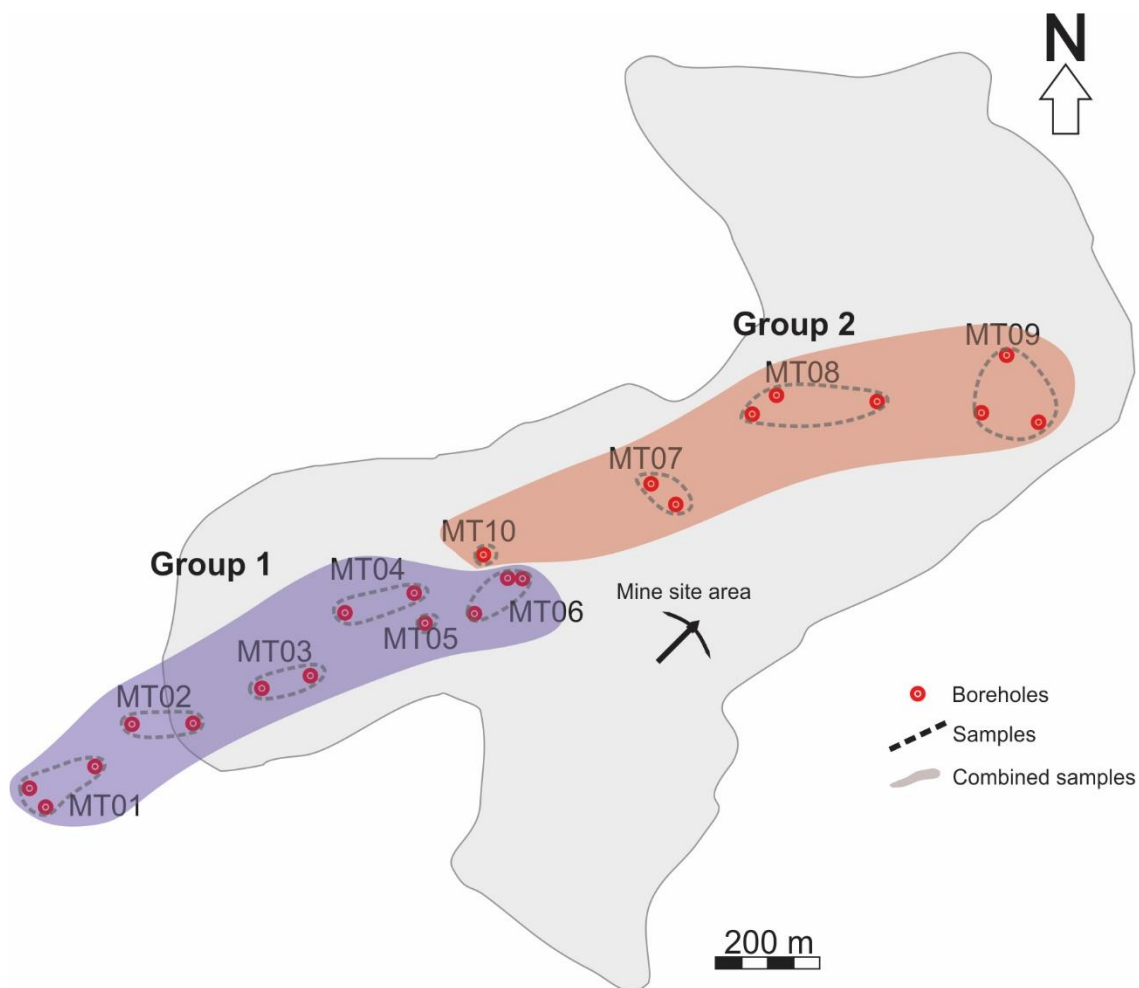
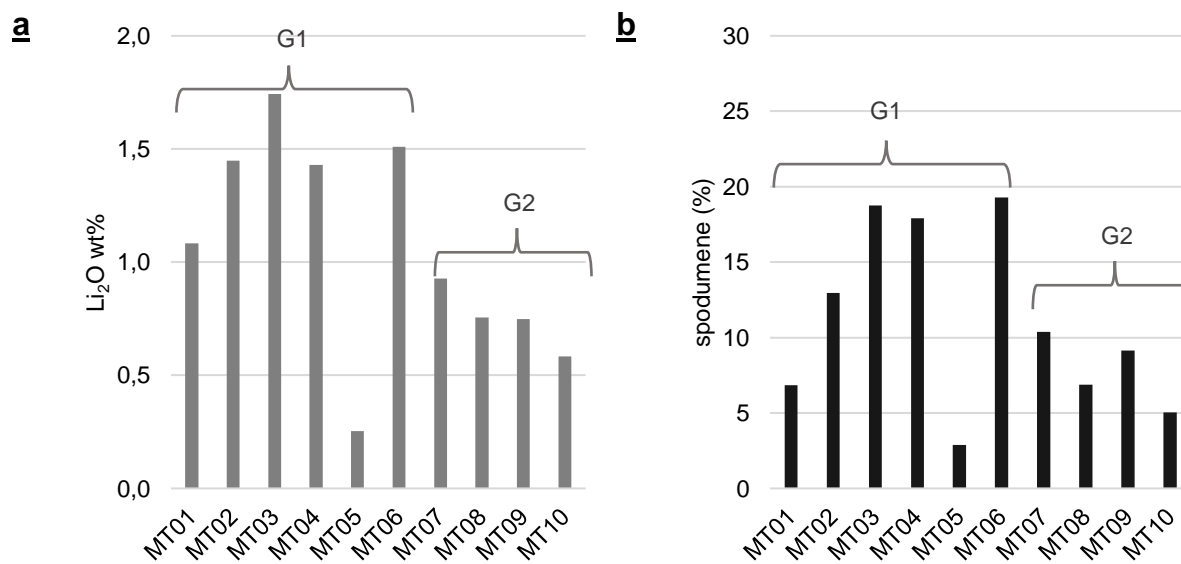
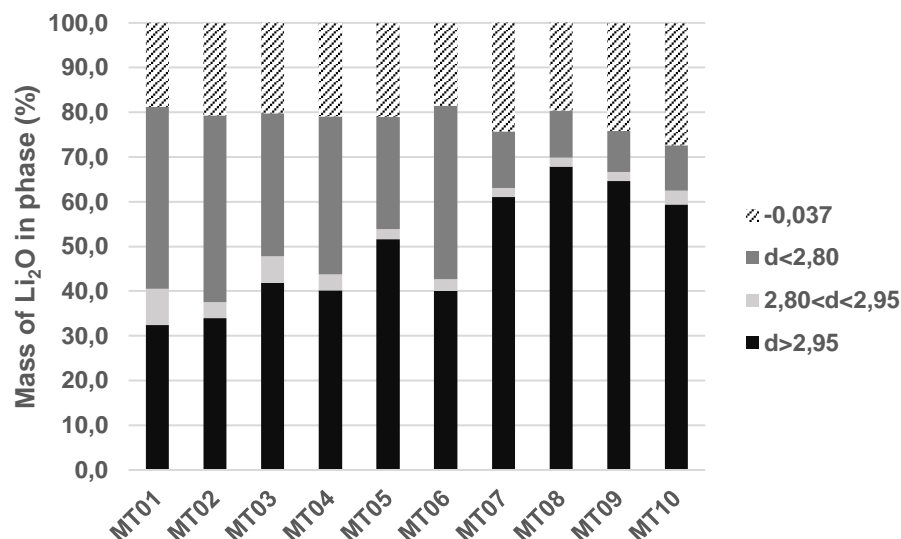
Figure 11 - Bulk Li_2O wt% content in samples (a) and spodumene content in the $-0.30 + 0.037$ mm size fraction (b).

Figure 12 - Lithium department in the heavy liquid separation



4.3 Detailed process mineralogy

This sector presents the results for the detailed process mineralogy study performed in G1 and G2.

4.3.1 Chemical Analysis

Table 9 shows the chemical composition of G1 and G2. Li₂O content in G1 is 1.26 wt%, whereas in G2 is 0.62 wt%. G1 contains lower Fe₂O₃ (0.32 wt%), CaO (0.43 wt%) and MgO (<0.10 wt%) contents then G2 (Fe₂O₃ 0.75 wt%, CaO 0.76 wt%, MgO 0.2 wt%). Contents of SiO₂, Al₂O₃, Na₂O and K₂O are similar in both samples, ~ 73.5 wt%, ~ 15.1 wt%, ~ 4.2 wt% and ~ 1.70 wt%, respectively.

Table 9 - Bulk chemical analysis.

Elemento	LiO ₂	Fe ₂ O ₃	SiO ₂	Al ₂ O ₃	CaO	MgO	MnO	Na ₂ O	K ₂ O	LOI	Total
Group 1	1.26	0.32	73.0	15.6	0.43	<0.10	0.17	3.74	1.76	2.73	99.1
Group 2	0.62	0.74	74.0	14.5	0.76	0.20	0.11	4.56	1.55	2.36	99.4

4.3.2 Sieve analysis

In both samples, the sieve analysis indicates that ~ 73% of the mass is retained in fraction +0.037 mm, while ~ 27% reports to fraction -0.037 mm. The mass distribution percentage decreases in the middling fraction (-0.10 +0.074 mm) and

increases towards the finer fraction (-0.037 mm). This trend is also observed in all elemental distribution percentages (Figure 13 and Table 10).

The Li_2O content ranges between 1.09 and 1.45 wt% in G1 and 0.63 and 0.75 wt% in G2. In both groups, the highest Li_2O content is observed in fraction -0.21+0.15 mm, while the lowest content is observed in fraction -0.037 mm. The elemental distribution is similar in both groups, in general ~ 76% reports to the total +0.037 mm and 24% to fraction -0.037 mm.

The Fe_2O_3 content ranges between 0.49 and 0.26 wt% in G1 and 0.50 and 1.18 wt% in G2. The highest Fe_2O_3 content is observed in fraction -0.037 mm while the lowest content is observed in the total +0.037. The elemental distribution is similar in both groups, in general ~ 60% reports to the total +0.037 mm and 40% to the finer fraction -0.037 mm. The CaO content and elemental distribution is similar to the observed for Fe_2O_3 , and both elements have the highest distribution in the finer size fractions (Figure 13).

The SiO_2 in both groups ranges between 70 and 75 wt% and in the elemental distribution approximately 74% reports to the total +0.037 mm size fractions. The Al_2O_3 in both groups ranges between 13 and 16 wt% and in the elemental distribution approximately 71% reports to the total +0.037 mm size fractions. The K_2O in both groups ranges between 1.6 and 2.1 wt% and in the elemental distribution approximately 74% reports to the total +0.037 mm size fractions.

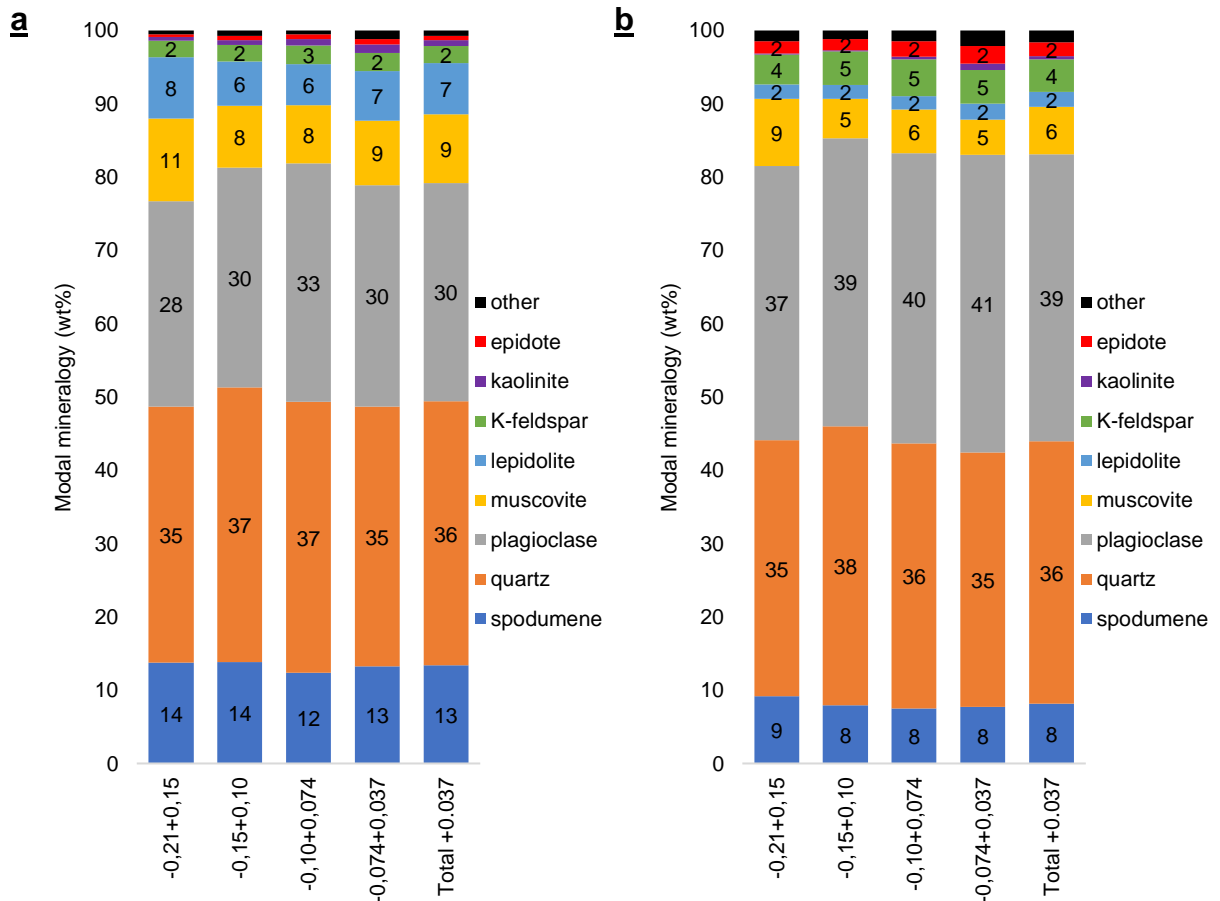
4.3.3 Mineral Composition

Figure 14a shows the mineral composition of Group 1, which is composed of: spodumene (~ 13%), quartz (~ 36%), plagioclase (~ 30%), muscovite (~9%), lepidolite (~7%), and K-feldspar (~2%).

Figure 14b shows the mineral composition of Group 2, which is composed of: spodumene (~ 8%), quartz (~ 36%), plagioclase (~ 39%), muscovite (~6%), Li-mica (~2%) and K-feldspar (~ 4%) the main components.

Group 2 has ~ 5% less spodumene, ~3% less muscovite, and ~5% less lepidolite than Group 1. On the other hand, Group 2 has ~ 9% more plagioclase and ~ 3% more K-feldspar than Group 1.

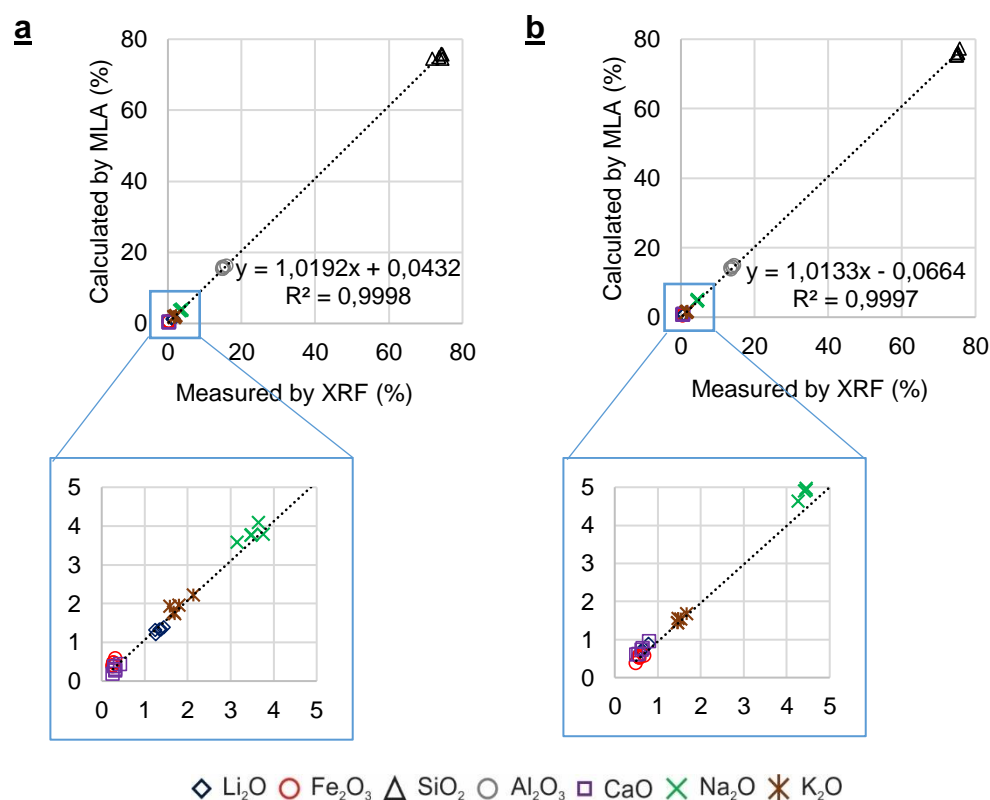
Figure 14 - Modal mineralogy of MLA measurements for Group 1 (a) and Group 2 (b).



*other: garnet, amphibole, apatite, cassiterite, microlite, coltan

The reliability of the reported data was verified considering reconciliation of the chemical results assayed by XRF and ICP-OES against those calculated by MLA based on modal mineralogy (Figure 15).

Figure 15 - Comparison of sample chemistry calculated by MLA and measured by XRF* for G1 (a) and G2 (b).



*Li₂O quantified using ICP-OES

4.3.4 Spodumene Characteristics

Figure 16 shows representative mineral composition maps of Group 1 in fraction -0.21+0.15 mm (Figure 16a, c, e) and a close up of spodumene grain associations with other minerals (Figure 16b, d, f). Group 1 is abundant in liberated spodumene grains often showing a tabular shape and quartz, plagioclase, muscovite, and lepidolite are generally present. The close up images show associations spodumene grains with plagioclase (Figure 16b) and muscovite (Figure 16d, f). Lepidolite appears to occur mainly along the margins and fractures of spodumene grains.

Figure 16 - MLA mineral composition map showing liberated spodumene bearing and gangue mineral particles in the +0.15 mm size fraction for Group 1 (a, c, e). The mineral maps on the right-hand side show close up of the different mineral textures in some spodumene grains (b, d, f).

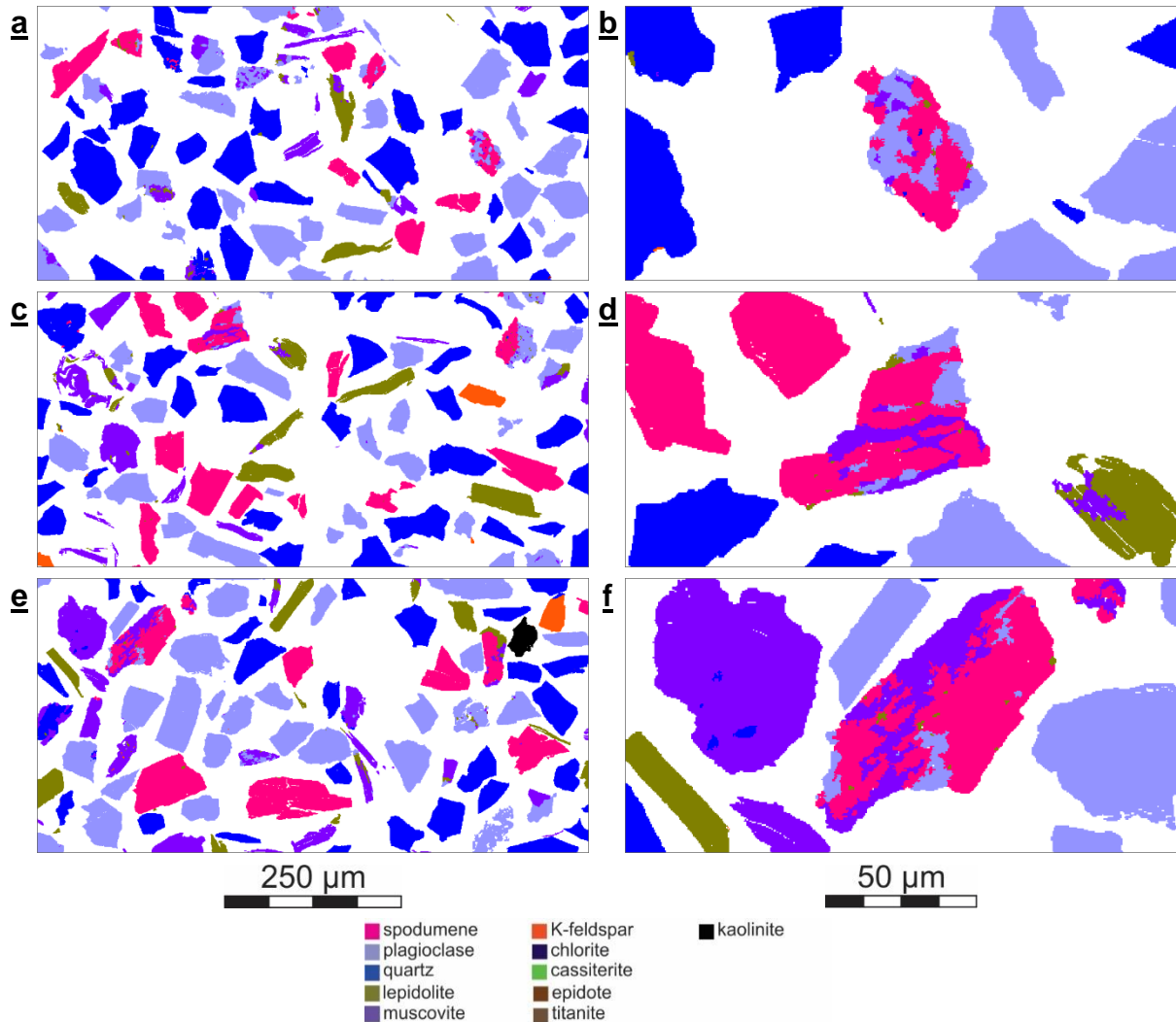


Figure 17 shows representative mineral compositional maps of Group 2 in fraction -0.21+0.15 mm (Figure 17a, c, e) and a close up of spodumene grain associations with other minerals (Figure 17b, d, f). Group 2 is also abundant in liberated spodumene particles often showing a tabular shape and quartz, plagioclase, muscovite, and lepidolite and K-feldspar are generally present. The close up images show spodumene grains associated with muscovite (Figure 17b) and plagioclase (Figure 17d, f).

Figure 17 - MLA mineral composition map showing liberated spodumene bearing and gangue mineral particles in fraction $-0.21+0.15$ mm for Group 2 (a. c. e). The mineral maps on the right-hand side show close up of the different mineral textures in some of the spodumene grains (b. d. f).

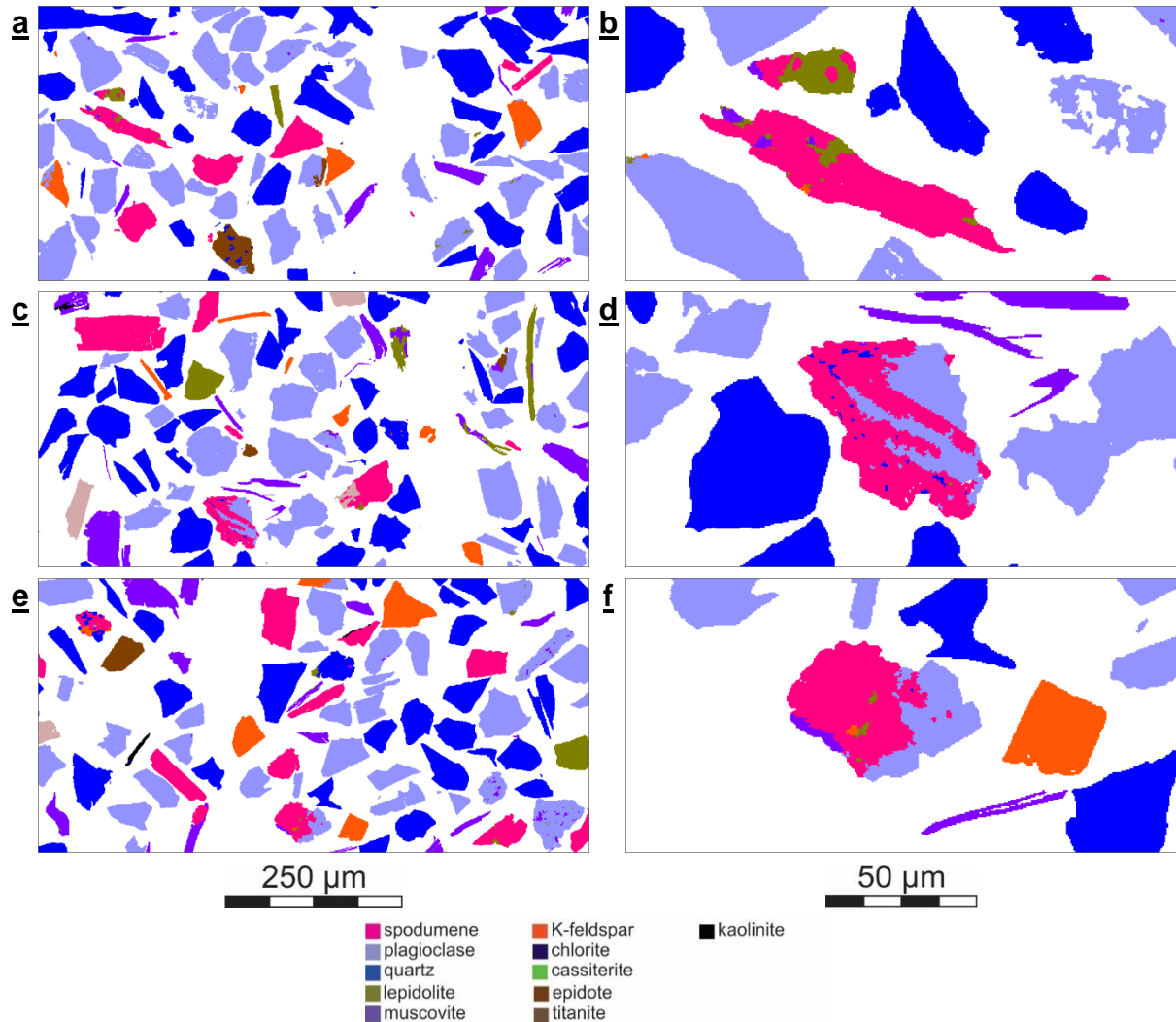


Table 11 shows a summary of the mineral locking aspects of spodumene particles in terms of liberated, binary, and complex spodumene particles for all size fractions in G1. Liberated particles are composed of >95% of spodumene in area.

The global liberation of spodumene (total $+0.037$ mm) is 89%, varying from 87% in the coarser size fraction to 94% in the smaller size fraction. Binary particles are more common than complex particles, they account for ~ 9% while complex particles account for ~ 2%. The most associations either binary or complex are with mica (muscovite + lepidolite), plagioclase and quartz.

Table 11 - Association characteristics of spodumene in Group 1.

Summary of spodumene association characteristics (wt%)							
Size fraction (mm)	Liberated	Binary	Complex	Binary + complex	Total		
-0.21+0.15	87	10	3	13	100		
-0.15+0.10	88	10	2	12	100		
-0.10+0.074	88	11	1	12	100		
-0.074+0.037	94	5	1	6	100		
Total +0.037	89	9	2	11	100		

Spodumene association characteristics in binary particles (wt%)							
Size fraction (mm)	quartz	plagioclase	K-feldspar	mica**	epidote	Kaolinite	other*
-0.21+0.15	1.4	2.8	0.5	5.1	0.0	0.1	0.1
-0.15+0.10	3.0	2.3	0.5	4.3	0.0	0.0	0.1
-0.10+0.074	2.9	2.9	0.1	4.9	0.0	0.2	0.4
-0.074+0.037	1.2	0.9	0.3	2.7	0.0	0.1	0.1
Total +0.037	1.9	2.2	0.4	4.2	0.0	0.1	0.1

Spodumene association characteristics in complex particles (wt%)							
Size fraction (mm)	quartz	plagioclase	K-feldspar	mica**	epidote	Kaolinite	other*
-0.21+0.15	0.7	1.3	0.2	1.1	0.0	0.0	0.0
-0.15+0.10	0.2	0.8	0.1	0.9	0.0	0.0	0.0
-0.10+0.074	0.2	0.4	0.1	0.3	0.0	0.0	0.0
-0.074+0.037	0.1	0.4	0.1	0.4	0.0	0.0	0.0
Total +0.037	0.3	0.8	0.1	0.7	0.0	0.0	0.0

*other: garnet. amphibole. apatite. cassiterite. microlite. coltan. **mica: muscovite + lepidolite

Table 12 shows a summary of the mineral locking aspects of spodumene particles in terms of liberated, binary, and complex spodumene particles for all size fractions in G2.

The global liberation of spodumene (total +0.037 mm) is 88%, varying from 86% in the coarser size fraction to 91% in the smaller size fraction. Binary particles are more common than complex particles, they account for ~ 10% while complex particles account for ~ 2%. The most associations either binary or complex are with plagioclase, mica (muscovite + lepidolite), and quartz.

Table 12 - Association characteristics of spodumene in Group 2.

Summary of spodumene association characteristics (wt%)							
Size fraction (mm)	Liberated	Binary	Complex	Binary + complex	Total		
-0.21+0.15	86	11	3	14	100		
-0.15+0.10	88	10	1	12	100		
-0.10+0.074	89	10	1	11	100		
-0.074+0.037	91	8	1	9	100		
Total +0.037	88	10	2	12	100		

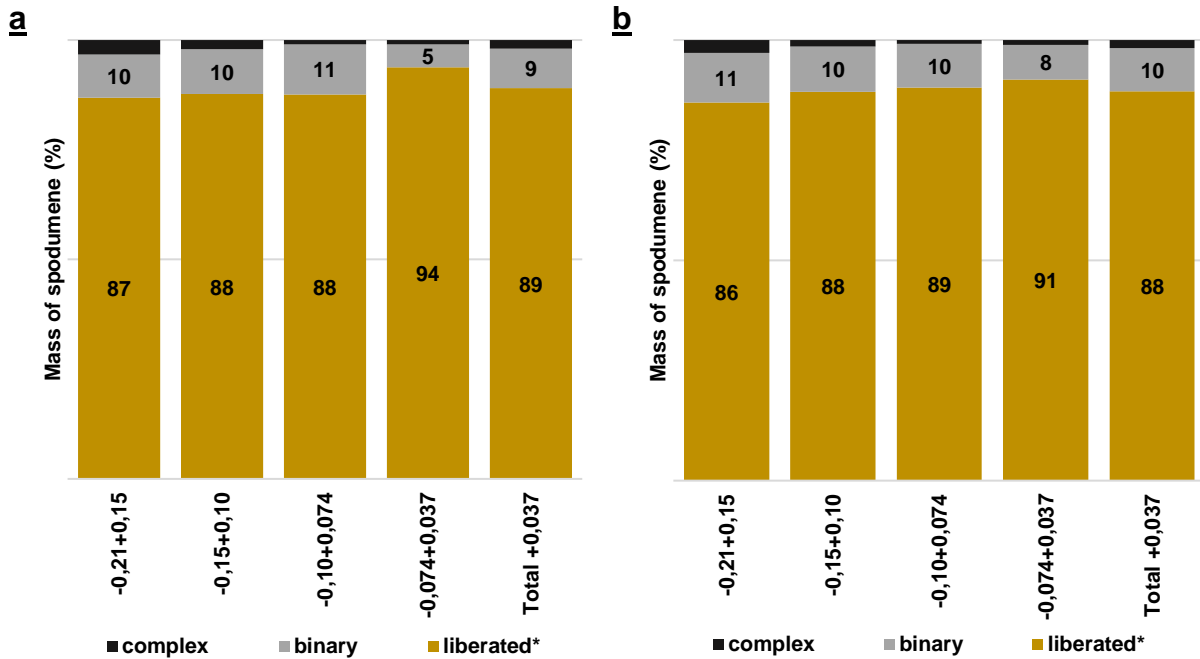
Spodumene association characteristics in binary particles (wt%)							
Size fraction (mm)	quartz	plagioclase	K-feldspar	mica**	epidote	Kaolinite	other*
-0.21+0.15	1.6	4.4	0.6	4.0	0.0	0.0	0.2
-0.15+0.10	3.9	3.8	0.2	1.9	0.0	0.0	0.5
-0.10+0.074	3.0	3.0	0.3	2.6	0.0	0.0	1.1
-0.074+0.037	1.9	1.9	0.1	2.7	0.2	0.2	0.7
Total +0.037	2.4	3.3	0.3	3.0	0.0	0.1	0.5

Spodumene association characteristics in complex particles (wt%)							
Size fraction (mm)	quartz	plagioclase	K-feldspar	mica**	epidote	Kaolinite	other*
-0.21+0.15	0.7	1.0	0.2	1.1	0.0	0.0	0.1
-0.15+0.10	0.3	0.4	0.1	0.5	0.0	0.0	0.1
-0.10+0.074	0.1	0.1	0.2	0.3	0.0	0.0	0.0
-0.074+0.037	0.2	0.6	0.2	0.3	0.0	0.0	0.0
Total +0.037	0.4	0.7	0.2	0.6	0.0	0.0	0.1

*other: garnet, amphibole, apatite, cassiterite, microlite, coltan. **mica: muscovite + lepidolite

Figure 18 shows a graphic representation of spodumene mineral locking characteristics for Group 1 (Figure 18a) and Group 2 (Figure 18b).

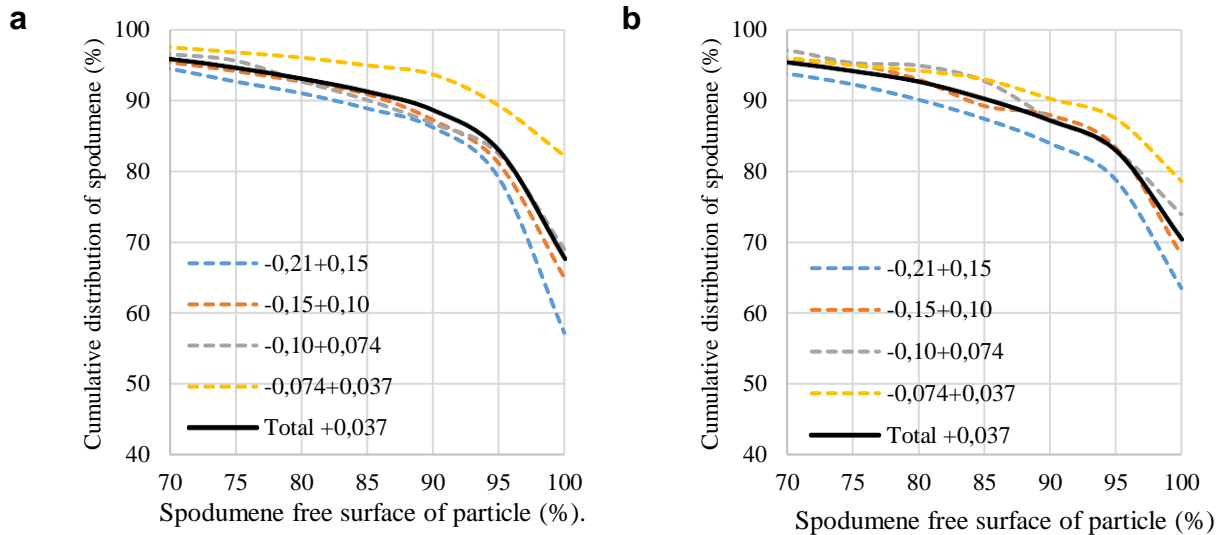
Figure 18 - Spodumene liberation characteristics for Group 1 (a) and Group 2 (b). Liberation is based on spodumene area (liberated $\geq 95\%$ spodumene). Binary particles are composed of spodumene and another mineral phase and complex particles are composed of spodumene and two or more different mineral phases.



*Liberated: Particles with spodumene area $\geq 95\%$

Figure 19a,b shows the liberation characteristics of spodumene for both groups in terms of liberated free surface area. In general, G2 shows slightly higher surface exposure than G1. In the Total +0.037 mm size fraction, spodumene particles with $\geq 95\%$ of free surface area represent approximately 83% in G1 and 87% in G2. Still considering particles with $\geq 95\%$ of free surface area, higher surface exposure is observed towards finer size fractions, only in this size fraction G1 has slightly higher surface exposure than G2.

Figure 19 - Mineral liberation by free surface area for spodumene in G1 (a) and G2 (b).



4.3.5 Mineral heavy liquid separation

4.3.5.1 Group 1

Table 13 shows the mineral heavy liquid separation test results performed in the fractions + 0.037 mm for Group 1. The floated products account for ~ 89% in mass of the test (~16% in mass of the samples). The sunken product accounts for ~ 11% in mass of the test (~ 2% of the samples).

In the total +0.037 mm product the Li_2O content in sunken product is 6.53 wt% and in the floated product the content is 0.62 wt%. The sunken product accounts for 57% in mass of the test (44% of the sample). Fe_2O_3 content in the sunken product is 0.76 wt% and in the floated product the content is 0.21 wt%. The sunken product accounts for 31% in mass of the test (19% of the test). The CaO content in the sunken product is 1.29 wt% and in the floated product 0.20 wt%. The sunken product accounts for 45% (26% of the sample).

In the total +0.037 mm product the SiO_2 , Al_2O_3 , Na_2O and K_2O contents are 75.6 wt%, 13.7 wt%, 3.71 wt% and 1.96 wt%. respectively. The sunken product of these elements account for 9%, 20%, 0.5% and 1.5% of the test (7.0%, 14%, 0.3%, 1.1% of the sample), respectively.

4.3.5.2 Group 2

Table 14 shows the mineral heavy liquid separation test results performed in the fractions + 0.037 mm for Group 2. The floated products account for ~ 90% in mass of the test (~20% in mass of the samples). The sunken products account for ~ 10% in mass of the test (~ 2% of the samples).

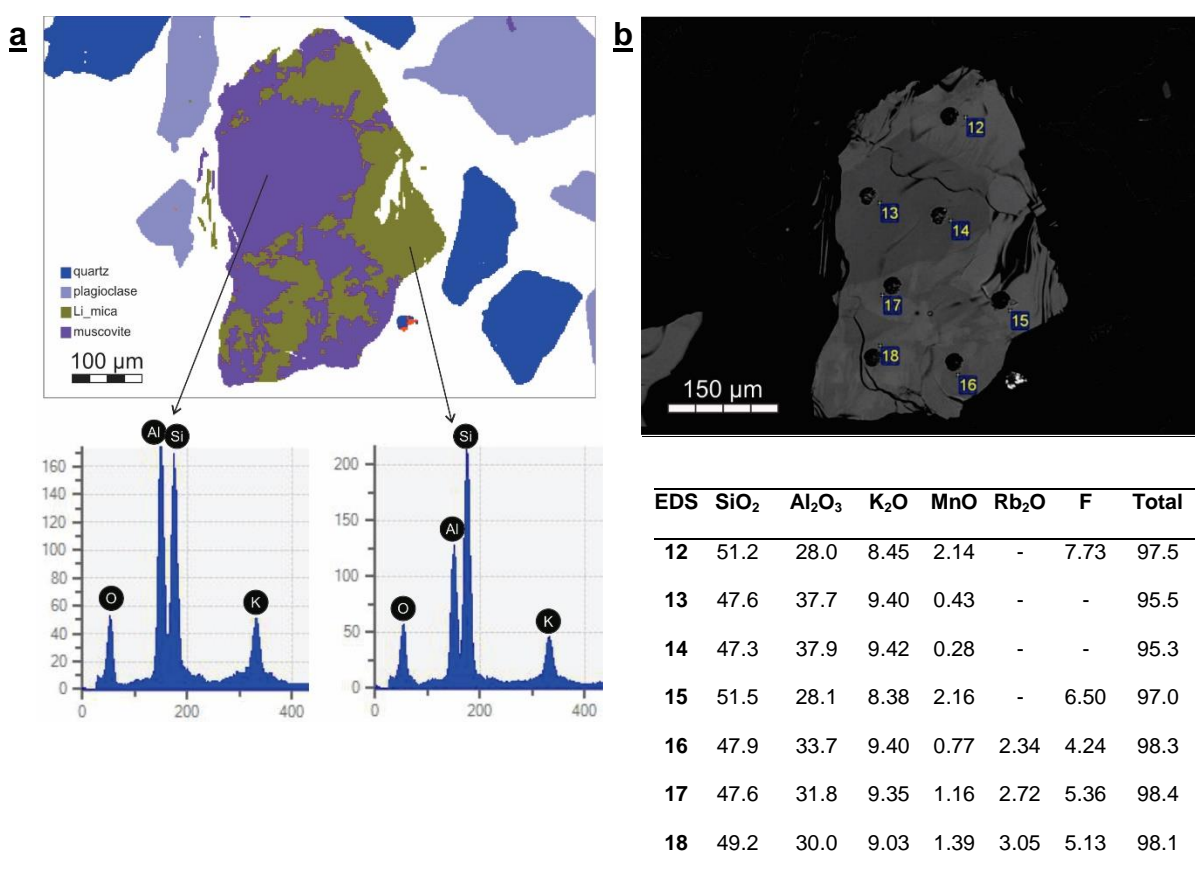
In the total +0.037 mm product the Li_2O content in sunken product is 4.92 wt% and in the floated product the content is 0.15 wt%. The sunken product accounts for 78% in mass of the test (58% of the sample). Fe_2O_3 content in the sunken product is 2.36 wt% and in the floated product the content is 0.39 wt%. The sunken product accounts for 40% in mass of the test (23% of the test). The CaO content in the sunken product is 4.0 wt% and in the floated product 0.25 wt%. The sunken product accounts for 64% (38% of the sample).

In the total +0.037 mm product the SiO_2 , Al_2O_3 , Na_2O and K_2O contents are 78.1 wt%, 12.8 wt%, 4.75 wt% and 1.65 wt%, respectively. The sunken product of these elements account for 7%, 17%, 0.5% and 1.6% of the test (5.5%, 12%, 0.3%, 1.2% of the sample), respectively.

4.3.6 Mica compositions

The mineralogy identified with MLA was able to distinguish two types of mica phases. Figure 20a shows a mineral composition map of a mica particle composed by the two types of micas and presents the differences of their X-ray spectra. Figure 20b shows a BSE image of the same mica particle and a table showing the EDS results for the different points analyzed in the particle. The purple phase, with lower gray scale and higher Al content was identified as muscovite, while the pale green phase, with brighter gray scale and lower Al content was identified as lepidolite.

Figure 20 - MLA mineral composition map of a mica particle showing the classification and the differences in X-ray spectra (a). BSE image and EDS analysis results table (b).



4.3.6.1 LA-ICPMS

To assess the presence of lithium in these micas, several grains of both groups have been analyzed using LA-ICPMS. The results show that muscovite has ~ 0.5 wt% Li₂O content (Table 15), while in lepidolite the content ranges from ~1 wt% up to almost

6 wt% Li₂O (Table 16). Also, both micas are enriched in Rb₂O, contents range from ~ 1 wt% to ~5 wt%.

Table 15 - Average composition of muscovite grains obtained by LA-ICPMS.

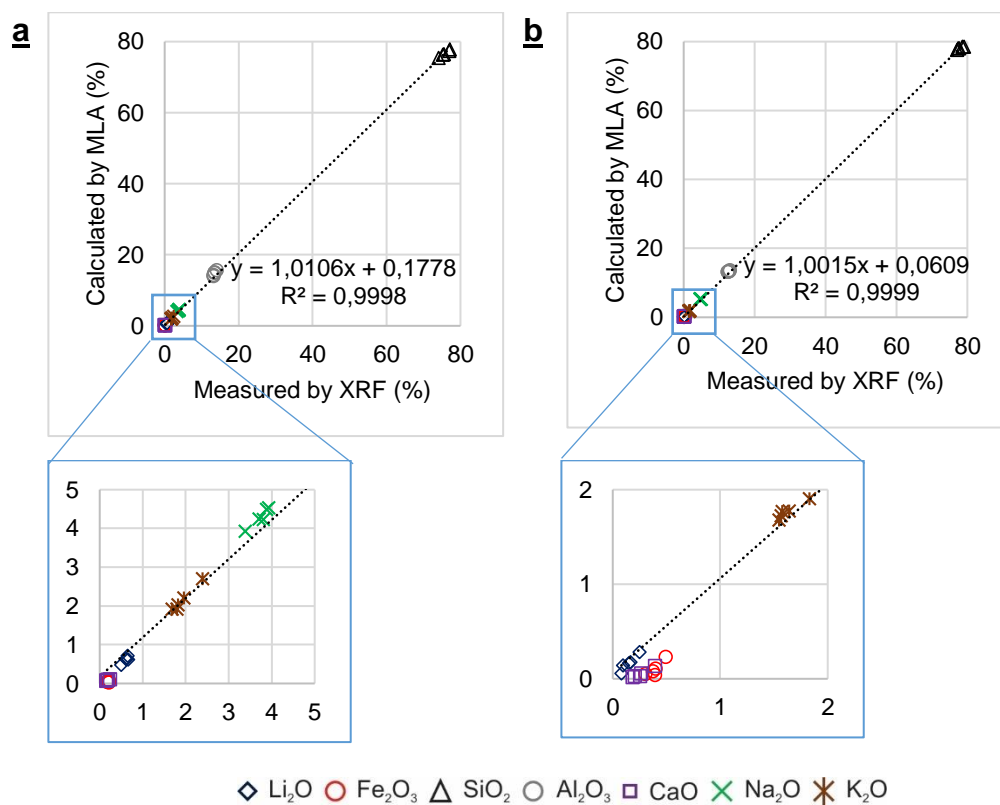
Muscovite	Li₂O	F	Al₂O₃	SiO₂	K₂O	FeO	Fe₂O₃	Rb₂O
Mean	0.48	0.22	36.87	46.98	10.14	2.33	2.61	3.25
SD	0.20	0.69	1.88	1.27	0.46	1.21	1.32	0.70
Max	0.95	2.78	40.83	50.28	11.17	5.47	6.08	4.23
Min	0.13	0.00	31.25	44.27	8.75	0.11	0.30	1.05

Table 16 - Average composition of lepidolite grains obtained by LA-ICPMS.

Lepidolite	Li₂O	F	Al₂O₃	SiO₂	K₂O	FeO	Fe₂O₃	Rb₂O
Mean	3.10	1.56	30.87	50.05	9.83	1.26	1.28	4.86
SD	1.34	2.83	3.47	2.81	0.60	1.89	2.15	0.95
Max	5.75	9.49	37.35	54.10	11.20	8.76	9.73	6.67
Min	1.25	0.00	24.01	44.78	8.93	0.24	0.00	2.65

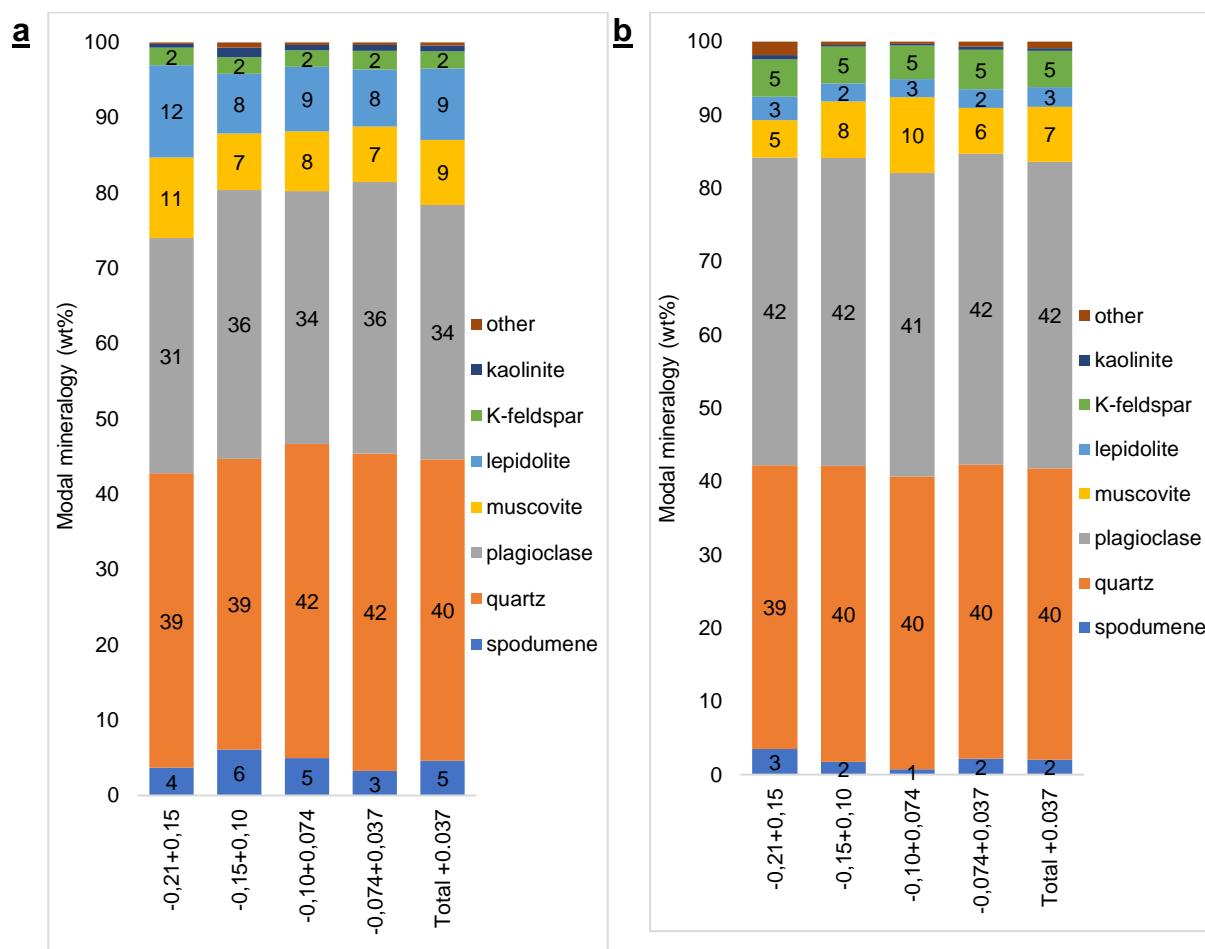
The reliability of the reported data was verified considering reconciliation of the chemical results assayed by XRF and ICP-OES against those calculated by MLA based on modal mineralogy of the floated products (Figure 21). Variations observed in some elements such as Fe, Ca and K in micas, were not modelled and account for variations in some values. The modal mineralogy obtained for the floated product and used in the reconciliation is shown in Figure 22.

Figure 21 - Comparison of sample chemistry by size fraction calculated by MLA and measured XRF* for the floated products of Group 1 (a) and Group 2 (b).



*Li₂O quantified using ICP-OES

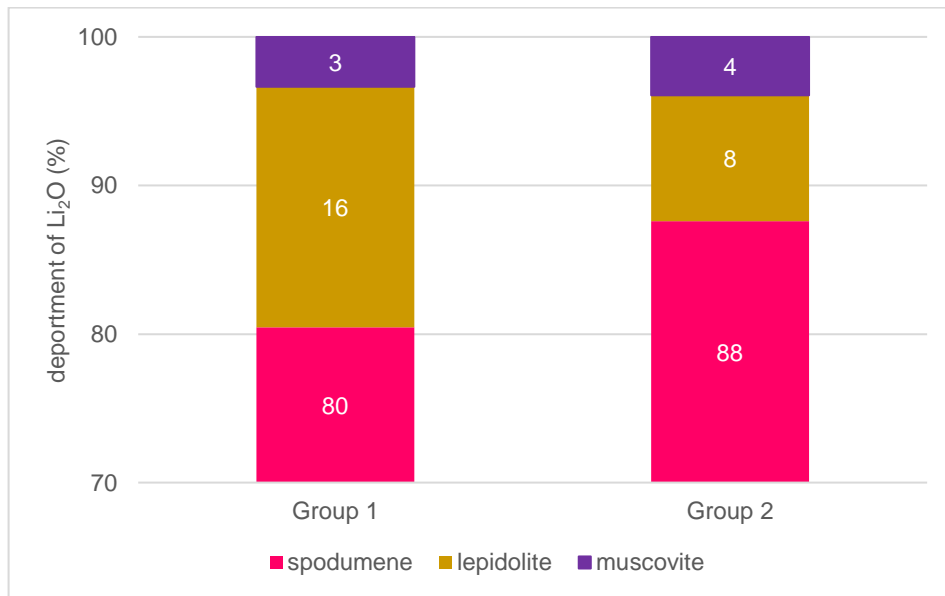
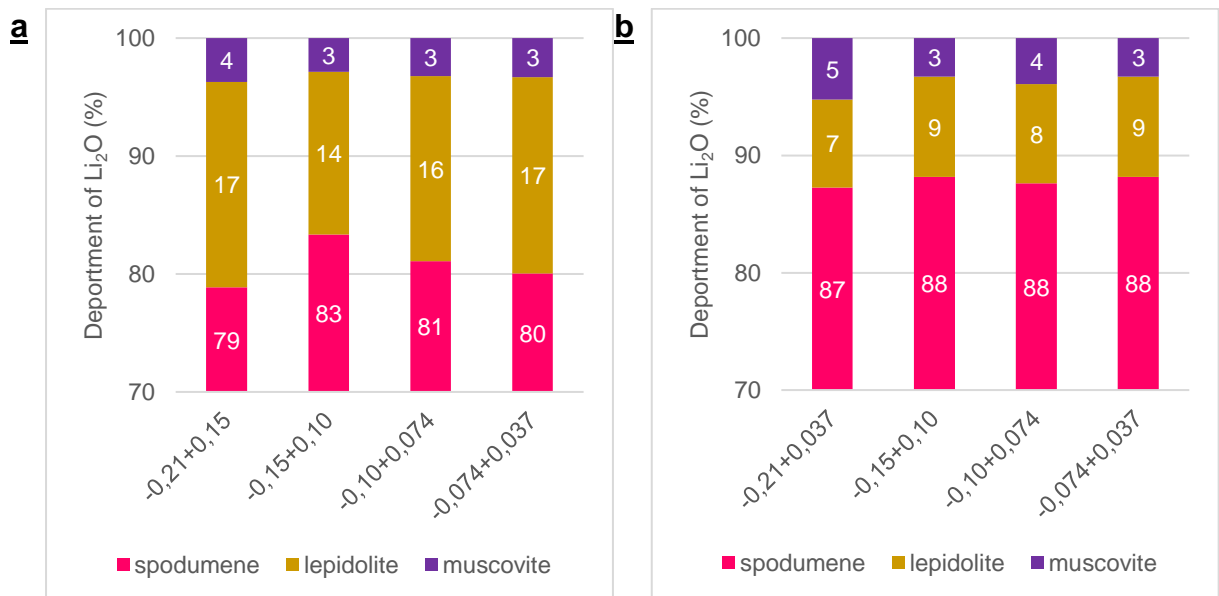
Figure 22 - Modal mineralogy by size fraction of the floated products for Group 1 (a) and Group 2 (b).



*other: garnet, amphibole, apatite, cassiterite, microlite, coltan, epidote

4.3.7 Lithium deportment

The Li deportment in the total +0.037 mm was calculated using the Li content evaluated by LA-ICPMS and relating the measured lithium concentrations in Li-containing minerals to the derived MLA modal abundance of the minerals in the samples. Figure 23 shows that most of the lithium is associated with spodumene. In Group 1, 80% of lithium is associated with spodumene, 16% with lepidolite and 3% with muscovite. In Group 2, 88% of lithium is associated with spodumene, 8% with lepidolite and 4% with muscovite. This tends to be similar in each size fraction of each group, respectively Figure 24.

Figure 23 - Li₂O department in the Total +0.037 mm size fraction.Figure 24 - Li₂O department by size fractions in Group 1 (a) and in Group 2 (b).

4.3.8 Grade-recovery

The Theoretical grade-recovery curve for spodumene in Group 1 (Figure 25) and Group 2 (Figure 26) indicate that at recoveries higher than 90%, higher spodumene grades are achieved in the finer fractions (-0.10+0.074 and -0.074 and -0.037 mm).

Figure 25 - Theoretical grade recovery curve for spodumene mineral grains in all studied size fractions of Group 1.

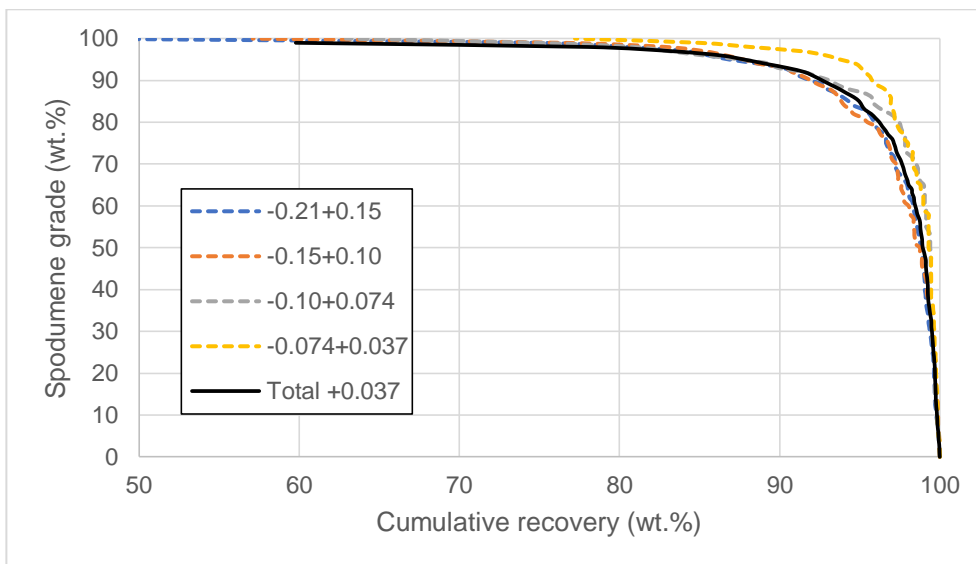
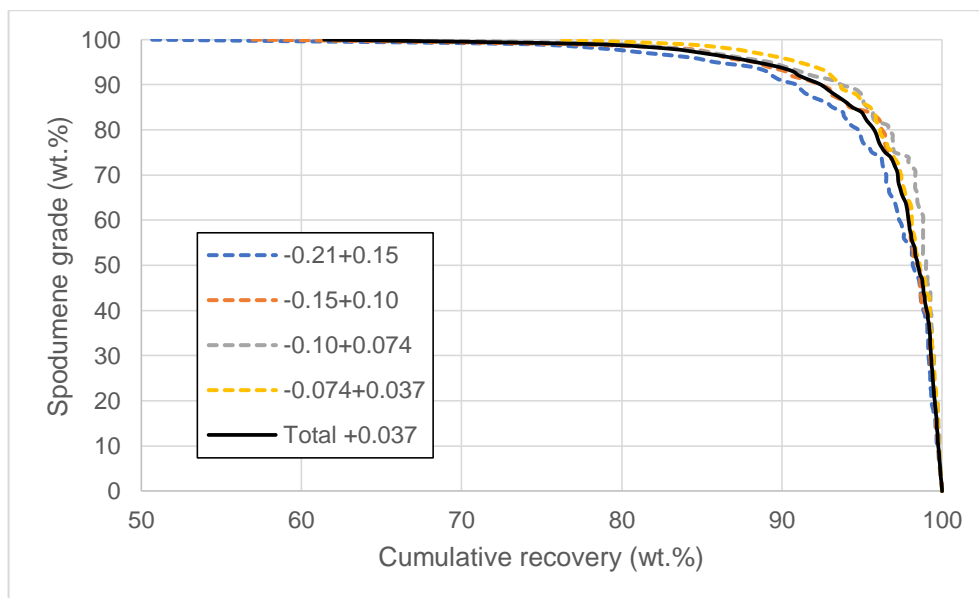


Figure 26 - Theoretical grade recovery curve for spodumene mineral grains in all studied size fractions of Group 2.

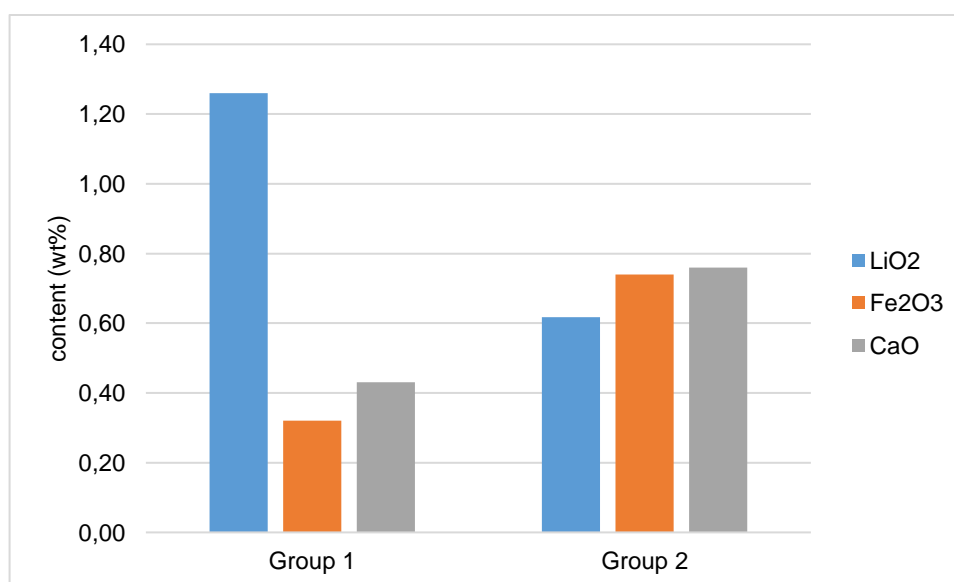


5 DISCUSSION

The broad ore characterization study revealed two sets of samples with similar behavior considering elemental and mineralogical composition, as well as heavy liquid separation test results, as shown in section 4.2. These two sets of samples have been combined and then submitted to the detailed process mineralogy study.

The detailed process mineralogy study showed that the bulk Li_2O content of Group 1 is 1.26 wt% which is similar to the content found in other pegmatite lithium deposits around the world. The Fe_2O_3 and CaO contents are low, which can be beneficial to the beneficiation process since iron-bearing minerals can be difficult to separate from spodumene using DMS or Flotation. On the other hand, Group 2 bulk Li_2O content is lower than the reported for most pegmatite deposits and Fe_2O_3 and CaO are almost twice as high as in Group 1.

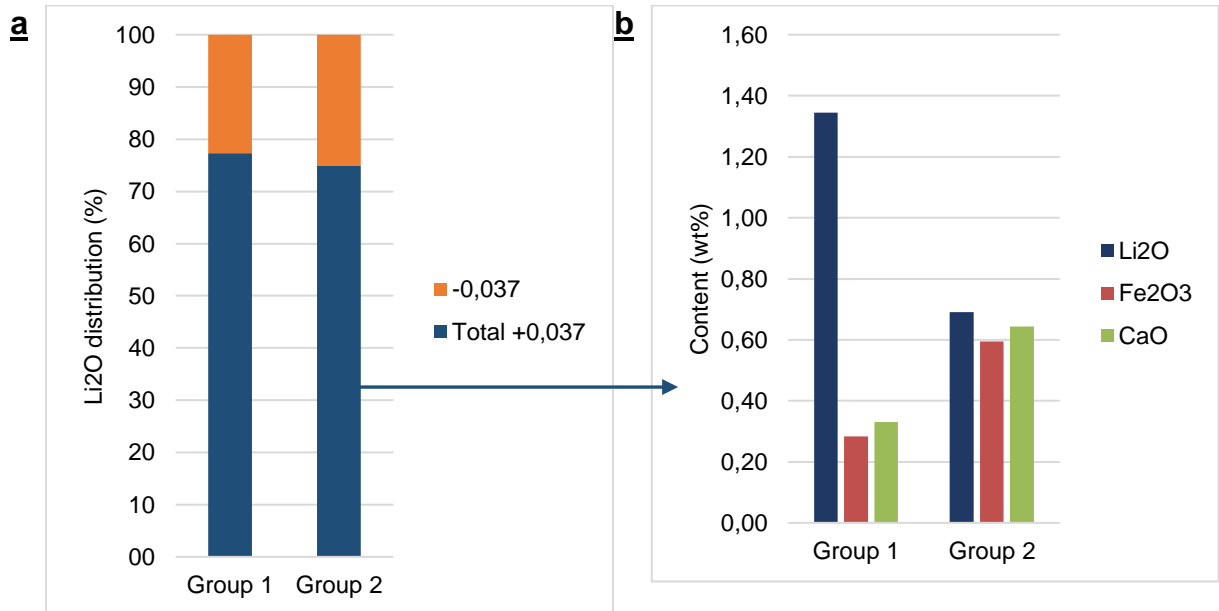
Figure 27 - Li_2O , Fe_2O_3 and CaO content in Group 1 and Group 2.



The sieve analysis shows that approximately 27% of the mass reports to the finer fraction (-0.037 mm) in both samples, and the Li_2O content in Group 1 is 1.09 wt% and 0.63 wt% in Group 2, accounting for 23% and 25% of lithium's department, respectively. In the Total $+0.037$ mm interval, the Li_2O content in Group 1 is 1.35 wt% and Group 2, 0.69 wt%, accounting for 77% and 75% of lithium's department,

respectively. The Fe_2O_3 content in this interval is three times higher and CaO content is two times higher in Group 2 (Figure 28a, b).

Figure 28 - Li_2O , Fe_2O_3 and CaO content in Total +0.037 mm size fraction of Group 1 and Group 2 (a). Li_2O distribution in the Total +0.037 mm and -0.037 mm size fractions for both Groups (b).

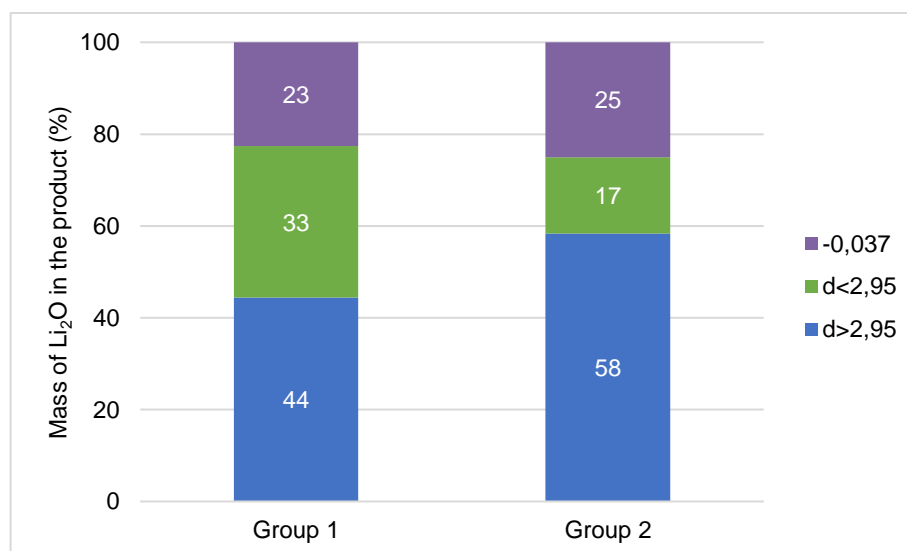


In term of mineralogical composition in the Total +0.037 size fraction, Group 1 has 5% more spodumene, 3% more muscovite and 5% more lepidolite. Group 2 has slightly more epidote and other minerals, which include iron-bearing minerals such as garnet and amphibole. The accuracy and consistency of the calculated MLA derived data are generally in good agreement with the chemical analysis performed in all size fractions, both samples present an R^2 value of 0.99.

The heavy liquid separation test results in the total+0.037 mm sunken product shows that Group 1 has higher lithium content (6.53 wt%) but lower lithium recoveries (44%) than Group 2. Group 2, on the other hand, has lower lithium content (4.92 wt%), but the distribution is higher in the sunken product (58%). Considering a target product of 6 wt% Li_2O and that distribution lies between 30 to 50% which is an acceptable range for industry (GRAMMATIKOPOULOS et al., 2021), Group 1 can potentially be beneficiated by DMS operation to obtain a technical grade product with low Fe_2O_3 grade (0.7 wt%). Group 2 on the other hand does not achieve minimum target grade of 6 wt% Li_2O and has high Fe_2O_3 content (2.3 wt%). Both products could be further

upgrade by performing magnetic separation to remove iron-bearing silicate minerals (epidote and amphibole).

Figure 29 - Lithium distribution in the heavy liquid separation test.



The difference in recoveries could be explained by the liberation degree of spodumene, but liberation characteristics show that both groups have high liberation degrees in the Total +0.037 mm size fraction: 89% for Group 1 and 88% for Group 2. Considering solely this liberation value (in area%) the lithium distribution in the sunken product should be much higher, around 90% instead of 44% or 58%, as observed in the heavy liquid separation test.

Different as in the Zoro pegmatite lithium project (GRAMMATIKOPOULOS et al., 2021) and in Pilangoora project (AYLMORE et al., 2018b) the presence of lithium-bearing micas (muscovite and lepidolite) did impact considerably the spodumene processing results. LA-ICPMS analysis showed that muscovite has Li_2O content of ~0.5 wt% and lepidolite ~3.1 wt%. Lepidolite represents a solid solution series intergrowth between the Al-bearing micas of polyolithionite and trilithionite, therefore the Li_2O content varies much, between 1.25 to 5.75 wt% Li_2O in the grains analyzed.

In the Total +0.037 mm size fraction the lithium content in spodumene account for 80% in Group 1 and 88% in Group 2. Thereby we can conclude the “real” head grade, which represent the Li_2O that can be recovered from spodumene. In Group 1, of the total Li_2O content (1.34 wt%), the “real” head grade is of ~1.0 wt% and in Group 2, of the total Li_2O content (0.69 wt%) the “real” head grade is of ~0.6%. These results

corroborate with J. WELHAM, 2019 statement that a spodumene pegmatite deposit where lithium is present at >10% in the minority phases (muscovite and lepidolite, in this work) it is more economically challenging because of the lower “real” head grade once the micas are eliminated.

In the heavy liquid separation results the lower distribution of lithium in Group 1 is due to the higher modal percentage of lepidolite that reports to the floated product and lowers the lithium distribution in the sunken product. The higher lithium content goes to the fact that Group 1 has lower modal presence of iron-bearing minerals that normally report to the sunken product and contaminates it with iron and calcium.

On the other hand, Group 2 has less modal percentage of lepidolite and therefore the lithium distribution is not so affected, maintaining most of the lithium within spodumene, which enriched the sunken product. Besides that, the lower lithium content is explained due to the higher modal presence of iron-bearing minerals (epidote and amphibole) in the sunken product that contaminates it with iron and calcium.

Considering the flotation process, the spodumene free surface has been evaluated and reveals higher liberation towards the finer size fractions. In the Total +0.037 mm at free surface of 95% distribution reaches ~84% in Group 1 and ~88% in Group 2. The liberation by free surface is important for further processing because it provides information on the surface area available for a leaching solution to reach or collector/depressant to attach to the ore mineral.

Finally, micas have a considerable amount of Rb and could be further studied to determine their potential as a source of this element. The same enrichment has been observed in the Zoro Pegmatite in feldspar and micas (GRAMMATIKOPOULOS et al., 2021) and in Pilangoora project in feldspar and beryl (AYLMORE et al., 2018b).

6 CONCLUSION

Lithium enriched pegmatite samples have been assessed by a combination of analytical techniques and mineral separations. Results show two sets of samples with different processing behaviors and a process mineralogy study by size fraction revealed that the lithium distribution between Li-bearing minerals played a major role in the processing behavior.

Group 1, composed of sample MT01 to MT06, presents lower lithium distribution in the sunken product due to the higher modal content of lepidolite, which shifts lithium distribution to the floated product. Group 2, composed of sample MT07 to MT10, has lower lepidolite modal content and therefore performs better in the lithium distribution to the sunken product.

Theoretical grade distribution curves indicate that high grade spodumene concentrate can easily be achieved with recoveries of 90%, especially in the finer size fractions. Heavy liquid separation showed that Group 1 has can potentially be beneficiated by DMS but Group 2 not, due to low Li_2O content and high Fe_2O_3 content in the product. Even though, magnetic separation could be applied on both sunken products to improve the lithium content making them suitable for technical-grade or even chemical-grade lithium concentrate. Lepidolite could also be further assessed as a source of lithium (1.25 to 5.75 wt% Li_2O) and rubidium (2.65 to 6.67 wt% Rb).

7 BIBLIOGRAPHY

ALBEMARLE. **Spodumene Concentrate, SC 7.2 Premium**. 2017. Disponível em: <https://www.albemarle.com/storage/components/T402211.PDF>. Acesso em: 29 ago. 2020.

AMG. **Lithium Project Update**. 2017. Disponível em: <https://amg-nv.com/wp-content/uploads/AMG-Lithium-FINAL.pdf>. Acesso em: 10 jun. 2020.

ASSUMPÇÃO, Caymon de Siqueira. **Caracterização Mineralógica e Geoquímica do Pegmatito da Mina de Volta Grande, província Pegmatítica de São João Del Rei, Nazareno, Minas Gerais**. 2015. Universidade Federal de Ouro Preto, 2015. Disponível em: <http://www.repositorio.ufop.br/handle/123456789/5986>.

AYLMORE, Mark G. Assessment of Lithium Pegmatite Ore Bodies to Determine Their Amenability to Processing for the Extraction of Lithium. *In: GLOBAL CONFERENCE ON EXTRACTIVE METALLURGY THE MINERALS , METALS & MATERIALS SERIES 2018, Anais [...].* [s.l: s.n.] p. 2261–2279. DOI: 10.1007/978-3-319-95022-8_190.

AYLMORE, Mark G.; MERIGOT, Kelly; QUADIR, Zakaria; RICKARD, William D. A.; EVANS, Noreen J.; MCDONALD, Bradley J.; CATOVIC, Enej; SPITALNY, Peter. Applications of advanced analytical and mass spectrometry techniques to the characterisation of micaceous lithium-bearing ores. **Minerals Engineering**, v. 116, n. April 2017, p. 182–195, 2018. a. DOI: 10.1016/j.mineng.2017.08.004. Disponível em: <https://doi.org/10.1016/j.mineng.2017.08.004>.

AYLMORE, Mark G.; MERIGOT, Kelly; RICKARD, William D. A.; EVANS, Noreen J.; MCDONALD, Bradley J.; CATOVIC, Enej; SPITALNY, Peter. Assessment of a spodumene ore by advanced analytical and mass spectrometry techniques to determine its amenability to processing for the extraction of lithium. **Minerals Engineering**, v. 119, p. 137–148, 2018. b. DOI: 10.1016/j.mineng.2018.01.010.

BALE, M. D.; MAY, A. V. Processing of ores to produce tantalum and lithium. **Minerals Engineering**, v. 2, n. 3, p. 299–320, 1989. DOI: 10.1016/0892-6875(89)90001-0.

BROWN, Teresa; WALTER, Abi; IDOINE, Naomi; GUNN, Gus; SHAW, Richard A.; RAYNER, Debbie. **Lithium British Geological Survey**. Keyworth. Disponível em: www.MineralsUK.com.

BULATOVIC, Srdjan M. Beneficiation of Lithium Ores. *In: Handbook of Flotation Reagents: Chemistry, Theory and Practice*. Peterborough: Elsevier B.V., 2015. p. 41–56. DOI: 10.1016/B978-0-444-53083-7.00003-8.

CBL. **Produção de compostos de lítio no Brasil**. 2016. Disponível em: https://www.cetem.gov.br/images/eventos/2016/ii_litio_brasil/apresentacoes/6-producao_de_compostos_de_litio_br.pdf. Acesso em: 9 jun. 2020.

CERNY, Petr; ERCIT, T. Scott. The classification of granitic pegmatites revisited. **The Canadian Mineralogist**, v. 43, n. 6, p. 2005–2026, 2005. DOI: 10.2113/gscanmin.43.6.2005.

CHRISTMANN, Patrice; GLOAGUEN, Eric; LABBÉ, Jean François; MELLETON, Jérémie; PIANTONE, Patrice. **Global Lithium Resources and Sustainability Issues**. DOI: 10.1016/B978-0-12-801417-2.00001-3.

EVANS, Keith. Lithium. *In: Critical Metals Handbook*. DOI: 10.1002/9781118755341. Disponível em: <http://doi.wiley.com/10.1002/9781118755341>.

FANDRICH, Rolf; GU, Ying; BURROWS, Debra; MOELLER, Kurt. Modern SEM-based mineral liberation analysis. **International Journal of Mineral Processing**, 2007. DOI: 10.1016/j.minpro.2006.07.018.

GARCIA, Ivan Jorge. **Sumário Mineral**. Brasília.

GARRETT, Donald E. **Handbook of Lithium and Natural Calcium Chloride Uses and Properties**. Elsevier B.V., 2004.

GIBSON, C.; AGHAMIRIAN, M.; GRAMMATIKOPOULOS, T. The beneficiation of lithium minerals from hard rock deposits. **Mining Engineering**, Denver, CO, v. 69, n. 8, p. 18–37, 2017.

GRAMMATIKOPOULOS, Tassos; AGHAMIRIAN, Massoud; FEDIKOW, Mark; MAYO, Toby. Mineralogical Characterization and Preliminary Beneficiation of the Zoro Lithium Project, Manitoba, Canada. **Mining, Metallurgy and Exploration**, v. 38, n. 1, p. 329–346, 2021. DOI: 10.1007/s42461-020-00299-2.

GRUBER, Paul W.; MEDINA, Pablo A.; KEOLEIAN, Gregory A.; KESLER, Stephen E.; EVERSON, Mark P.; WALLINGTON, Timothy J. Global lithium availability: A constraint for electric vehicles? **Journal of Industrial Ecology**, v. 15, n. 5, p. 760–775, 2011. DOI: 10.1111/j.1530-9290.2011.00359.x.

HENLEY, K. J. **Ore-Dressing Mineralogy**, 1986.

HOCKING, Mathew; KAN, James; YOUNG, Paul; TERRY, Chris; BEGLEITER, David. **Lithium 101**. Disponível em: <http://www.metalstech.net/wp-content/uploads/2016/07/17052016-Lithium-research-Deutsche-Bank.compressed.pdf>.

J. WELHAM, Nicholas. Lithium. *In: DUNNE, Robert C.; KAWATRA, Komar S.; YOUNG, Courtney A. (org.). SME Mineral Processing and Extractive Metallurgy Handbook*. Englewood: Society for Mining, Metallurgy & Exploration (SME), 2019. p. 1839–1853.

JASKULA, Brian W. **U.S. Geological Survey, Mineral Commodity Summaries**.

JASKULA, Brian W. **U.S. Geological Survey, Mineral Commodity Summaries**. DOI: 10.1017/CBO9781107415324.004.

KAVANAGH, Laurence; KEOHANE, Jerome; CABELLOS, Guiomar Garcia; LLOYD, Andrew; CLEARY, John. Global lithium sources-industrial use and future in the electric vehicle industry: A review. **Resources**, v. 7, n. 3, 2018. DOI: 10.3390/resources7030057.

LI, Huan; EKSTEEN, Jacques; KUANG, Ge. Recovery of lithium from mineral resources: State-of-the-art and perspectives – A review. **Hydrometallurgy**, v. 189, n. March, p. 105129, 2019. DOI: 10.1016/j.hydromet.2019.105129. Disponível em: <https://doi.org/10.1016/j.hydromet.2019.105129>.

LONDON, David. Ore-forming processes within granitic pegmatites. **Ore Geology Reviews**, v. 101, n. April, p. 349–383, 2018. DOI: 10.1016/j.oregeorev.2018.04.020. Disponível em:

<https://doi.org/10.1016/j.oregeorev.2018.04.020>.

LOTTER, Norman O. Review of evaluation models for the representative sampling of ore. **The South African Institute of Mining and Metallurgy**, n. August, p. 149–156, 1995.

LOTTER, Norman O. Modern Process Mineralogy: An integrated multi-disciplined approach to flowsheeting. **Minerals Engineering**, v. 24, n. 12, p. 1229–1237, 2011. DOI: 10.1016/j.mineng.2011.03.004. Disponível em: <http://dx.doi.org/10.1016/j.mineng.2011.03.004>.

MARTIN, Gunther; RENTSCH, Lars; HÖCK, Michael; BERTAU, Martin. Lithium market research – global supply, future demand and price development. **Energy Storage Materials**, v. 6, n. August 2016, p. 171–179, 2017. DOI: 10.1016/j.ensm.2016.11.004. Disponível em: <http://dx.doi.org/10.1016/j.ensm.2016.11.004>.

MCLENNAN, S. M. Relationships between the trace element composition of sedimentary rocks and upper continental crust. **Geochemistry, Geophysics, Geosystems**, v. 2, n. 4, 2001. DOI: 10.1029/2000GC000109.

MESHARAM, Pratima; PANDEY, B. D.; MANKHAND, T. R. Extraction of lithium from primary and secondary sources by pre-treatment, leaching and separation: A comprehensive review. **Hydrometallurgy**, v. 150, p. 192–208, 2014. DOI: 10.1016/j.hydromet.2014.10.012. Disponível em: <http://dx.doi.org/10.1016/j.hydromet.2014.10.012>.

MUNSON, Gerald A.; CLARKE, Fremont F. Heavy-Media separation plant and mine area Mining and Concentrating Spodumene In the Black Hills, South Dakota. **Mining Engineering**, v. 202, n. November, p. 1041–1045, 1955. Disponível em: <https://www.911metallurgist.com/blog/wp-content/uploads/2016/05/Extraction-of-Lithium-from-lts-Ores.pdf>.

NASCIMENTO, Marisa; SANTOS, Ronaldo L.; BRAGA, Paulo F. A.; FRANÇA, Sílvia C. A. **Recursos Minerais no Brasil Minerais estratégicos : terras raras e lítio**.

OLIAZADEH, M.; AGHAMIRIAN, M.; ALI, S.; LEGAULT, E.; GIBSON, C. Flowsheet Development for Beneficiation of Lithium Minerals from Hard Rock Deposits. *In: GLOBAL CONFERENCE ON EXTRACTIVE METALLURGY THE MINERALS , METALS & MATERIALS SERIES 2018, Anais [...].* [s.l: s.n.] p. 2293–2307. DOI: 10.1007/978-3-319-95022-8_192.

PAES, Vinícius J. C.; SANTOS, Luana D.; TEDESCHI, Mahyra F.; BETIOLLO, Leandro M. **Avaliação do potencial do lítio no Brasil: área do Médio Rio Jequitinhonha, nordeste de Minas Gerais**.

SANDMANN, Dirk; GUTZMER, Jens. Use of Mineral Liberation Analysis (MLA) in the Characterization of Lithium-Bearing Micaceous Minerals. **Journal of Minerals and Materials Characterization and Engineering**, v. 01, n. 06, p. 285–292, 2013. DOI: 10.4236/jmmce.2013.16043.

SWEETAPPLE, Marcus T.; TASSIOS, Steven. Laser-induced breakdown spectroscopy (LIBS) as a tool for in situ mapping and textural interpretation of lithium in pegmatite minerals. **American Mineralogist**, v. 100, n. 10, p. 2141–2151, 2015. DOI: 10.2138/am-2015-5165.

TADESSE, Bogale; MAKUEI, Fidele; ALBIJANIC, Boris; DYER, Laurence. The beneficiation of lithium minerals from hard rock ores : A review. **Minerals Engineering**, v. 131, n. September 2018, p. 170–184, 2019. DOI: 10.1016/j.mineng.2018.11.023. Disponível em: <https://doi.org/10.1016/j.mineng.2018.11.023>.

TRAN, Tam; LUONG, Van T. Lithium Production Processes. *In: Lithium Process Chemistry*. Gwangju: Elsevier Inc., 2015. p. 81–124. DOI: 10.1016/B978-0-12-801417-2.00003-7.

VINE, James D. Lithium Resources and Requirement by the Year 2000. **U.S. Geological Survey Professional Paper 1005**, 1976.

VON KNORRING, O.; CONDLIFFE, E. Mineralized pegmatites in Africa. **Geological Journal**, v. 22, n. 2 S, p. 253–270, 1987. DOI: 10.1002/gj.3350220619.